Effects of early marine diagenesis and site-specific depositional controls on carbonate-associated sulfate: insights from paired S and O isotopic analyses

Jocelyn A. Richardson[1*], Aivo Lepland[2,3], Olle Hints[3], Anthony R. Prave[4], William P. Gilhooly III[5], Alexander S. Bradley[1] and David A. Fike[1*]

[1]Department of Earth and Planetary Sciences, Washington University, St. Louis, MO 63130 USA

[2]Geological Survey of Norway, 7491 Trondheim, Norway

[3]Department of Geology, Tallinn University of Technology, Ehitajate 5, 19086 Tallinn, Estonia

[4]School of Earth and Environmental Sciences, University of St Andrews, Fife, KY16 9AL, Scotland

[5] Department of Earth Sciences, Indiana University-Purdue University Indianapolis, Indianapolis, IN, USA

[*]Corresponding authors:

E-mail: jocelynr@slac.stanford.edu. Phone: +1 (650) 926-5145

E-mail: dfike@levee.wustl.edu. Phone: +1 (314) 935-6607

Keywords: carbonate-associated sulfate, CAS, sulfur isotopes, sulfate oxygen isotopes, Ireviken bioevent, Silurian

This is the author's manuscript of the article published in final edited form as:

Richardson, J. A., Lepland, A., Hints, O., Prave, A. R., Gilhooly, W. P., Bradley, A. S., & Fike, D. A. (2021). Effects of early marine diagenesis and site-specific depositional controls on carbonate-associated sulfate: Insights from paired S and O isotopic analyses. Chemical Geology, 584, 120525. https://doi.org/10.1016/j.chemgeo.2021.120525

Abstract

Carbon, sulfur and oxygen isotope profiles in Silurian strata of the Baltoscandian Basin (Estonia), coincident with the Ireviken Bioevent, provide insights into basin-scale and platform-specific depositional processes. Paired carbon isotope records preserve a positive isotope excursion during the early Wenlock, coincident with faunal turnover, yet $\delta^{13}C$ variability of this excursion compared to other locations within the paleobasin reflects local depositional influences superimposed on a global signal. In comparison, sulfur isotope records do not preserve a systematic isotopic excursion over the same interval. Instead, sulfur isotope records have high sample-to-sample stratigraphic variability, particularly in shallow-water carbonate rocks (scatter up to ~10‰ for $\delta^{34}S_{CAS}$ and ~25‰ for $\delta^{34}S_{pyr}$). This pattern of isotopic variability is also found between sites from the same carbonate platform, where the magnitude and isotopic variability in $\delta^{34}S_{CAS}$ and $\delta^{34}S_{pyr}$ differ depending on relative local sea level (and therefore facies). Such facies-dependent variability reflects more closed- versus more open-system diagenetic conditions where pulses of increased sedimentation rate in the shallow water environments generates greater isotopic variability in both $\delta^{34}S_{CAS}$ and $\delta^{34}S_{pyr}$. Increased reworking and proximity to the shoreline results in local sulfide oxidation, seen as a decrease in $\delta^{34}S_{CAS}$ in the most proximal settings. Platform-scale evolution of isotopically distilled pore-fluids associated with dolomitization results in increased $\delta^{34}S_{CAS}$ in deep water settings. Correlations in paired $\delta^{34}S_{CAS}$-$\delta^{18}O_{CAS}$ data support these conclusions, demonstrating the local alteration of CAS during deposition and early marine diagenesis. We present a framework to assess the sequence of diagenetic and depositional environmental processes that have altered $\delta^{34}S_{CAS}$ and find that $\delta^{34}S$ of ~27-28‰ approximates Silurian seawater sulfate. Our findings provide a mechanism to understand the elevated variability in many deep-time $\delta^{34}S_{CAS}$ records that cannot otherwise be reconciled with behavior of the marine sulfate reservoir.

1.0 Introduction

The evolution of global biogeochemical cycles over Earth history is recorded in the chemical abundances and isotopic ratios of elements in marine sedimentary rocks (e.g. Bartley and Kah, 2004; Garrels and Lerman, 1981). The isotopic ratios of carbon and sulfur are particularly informative because values from both oxidized and reduced phases (carbonate, organic carbon, sulfate, sulfide) are preserved, and can be measured, in carbonate rocks. Changes in these isotopic ratios over time are typically inferred to represent perturbations to the carbon and sulfur cycles; efforts to understand the source of these perturbations have recognized the importance of deconvolving global versus local processes (Fike et al., 2015; Jones et al., 2019; Pasquier et al., 2017; Rose et al., 2019).

Variations in carbon isotope values ($\delta^{13}C$) of carbonate and organic carbon through time can be attributed to global carbon cycle perturbations (Kump and Arthur, 1999) and/or local processes, such as: facies changes (e.g. Rose et al., 2019), variations in productivity between deep- and shallow-marine settings and its effect on the dissolved inorganic carbon (DIC) pool (e.g. Jones et al., 2019; Swart and Eberli, 2005), changes in carbonate mineralogy, and sediment- versus fluid-buffered diagenesis (Higgins et al., 2018). Moreover, the stratigraphic expression of carbon isotope excursions can be variable in magnitude and duration between time-correlative sections (Jones et al., 2019; Samtleben et al., 2000), complicating efforts to understand the mechanism generating the $\delta^{13}C_{carb}$ signals.

Sulfur archives in the sedimentary record include oxidized sulfur in gypsum, anhydrite, barite (Paytan, 1998; Strauss, 1997) and carbonate-associated sulfate (CAS) (Burdett et al., 1989), as well as reduced sulfur sinks in pyrite and organic S compounds (Canfield, 2001). Microbial

65 sulfate reduction (MSR) can impart an isotopic fractionation that leaves the resultant product
66 sulfide depleted in ^{34}S relative to the sulfate pool by as much as 70‰ (Eldridge et al., 2016; Sim
67 et al., 2011). Due to the spatial and temporal extent of carbonate strata and their ability to preserve
68 sulfur isotope ($\delta^{34}S$) records of both CAS and pyrite, carbonate rocks have been investigated to
69 constrain the evolution of the global sulfur cycle.

70 Stratigraphic datasets of coeval pyrite and CAS $\delta^{34}S$ have traditionally been interpreted to
71 record changes to the global sulfur cycle, reflecting one or a combination of: changes to the burial
72 and weathering fluxes of pyrite and/or sulfate minerals, the size of the marine sulfate reservoir,
73 and/or the dominant microbial metabolic community and the associated biological fractionation
74 (Canfield, 2001; Garrels and Lerman, 1981). Recent studies aiming to reconstruct the ancient
75 sulfur cycle have generated highly variable, both regionally and stratigraphically, sulfur isotope
76 datasets in $\delta^{34}S_{pyr}$ and $\delta^{34}S_{CAS}$ (Jones and Fike, 2013; Thompson and Kah, 2012; Young et al.,
77 2016). Such large, commonly facies-dependent, variability in $\delta^{34}S_{pyr}$ (e.g. Richardson et al., 2019a;
78 Rose et al., 2019), is not unexpected as pyrite typically forms within sediments under evolving
79 diagenetic conditions. Moreover, there is a good framework in place to understand such variability
80 in terms of local environmental parameters, such as sedimentation rate and/or organic carbon
81 loading (Aller et al., 2010; Bryant et al., 2019; Claypool, 2004; Fike et al., 2015; Liu et al., 2019;
82 Pasquier et al., 2017). Yet the origin and environmental significance of variability in $\delta^{34}S_{CAS}$, often
83 interpreted to record global marine sulfate, remains poorly understood. Typical sample-to-sample
84 bulk rock $\delta^{34}S_{CAS}$ can vary as much as 10-12‰ within an individual stratigraphic section, which
85 is difficult to reconcile with the behavior of the marine sulfate reservoir unless the concentration
86 of seawater sulfate was very low (Fike et al., 2015). Interpretations of the source of this 'noise'
87 include basin- to global-scale sulfur cycle perturbations (Adams et al., 2010; Gill et al., 2007;

Kozik et al., 2019; Stebbins et al., 2018; Thompson and Kah, 2012) and locally variable depositional and early diagenetic environments (Present et al., 2019; Richardson et al., 2019a; Rose et al., 2019). To better understand the origin of this variability in $\delta^{34}S_{CAS}$, we seek additional information by measuring the oxygen isotopic composition in CAS.

Oxygen isotope values of sulfate ($\delta^{18}O_{SO4}$) are a supplementary proxy to interrogate the operation of the sulfur cycle. At normal seawater temperatures and pH, oxygen isotopes between sulfate and seawater require 10^{6-7} years to abiotically equilibrate (Chiba and Sakai, 1985). In the absence of diagenetic alteration and overprinting, $\delta^{18}O_{SO4}$ variability over longer geologic timescales will reflect changes in the major fluxes involving sulfate in the sulfur cycle, and $\delta^{18}O_{SO4}$ variability over shorter geologic timescales ($< 10^6$ years) reflects the dominant metabolisms within local microbial sulfur cycling (MSR, sulfide oxidation, sulfur disproportionation) and/or abiotic sulfide and pyrite oxidation (Bottrell and Newton, 2006; Turchyn and Schrag, 2006). Holding all other variables constant, MSR will result in an increase in paired $\delta^{34}S_{SO4}$-$\delta^{18}O_{SO4}$ values, while sulfide oxidation will be tracked as a coeval decrease in paired $\delta^{34}S_{SO4}$-$\delta^{18}O_{SO4}$ data (Goldberg et al., 2005). A decoupling of $\delta^{34}S_{SO4}$-$\delta^{18}O_{SO4}$ is generally understood to reflect differences in global vs. local influence on these isotope systems (Turchyn and Schrag, 2006). Consequently, paired $\delta^{34}S_{SO4}$-$\delta^{18}O_{SO4}$ and $\delta^{34}S_{SO4}$-$\delta^{34}S_{pyr}$ can be powerful tools for reconstructing the global and local sulfur cycles in ancient carbonate successions (Rennie and Turchyn, 2014).

We used the well-characterized Silurian stratigraphy of the East Baltic portion of the Baltoscandian Basin (e.g. Cramer et al., 2010; Hints et al., 2006; Kaljo and Martma, 2000; Kiipli et al., 2006, 2008; Loydell et al., 2010; Rose et al., 2019; Samtleben et al., 2000; Young et al., 2020) and $\delta^{13}C_{carb}$, $\delta^{13}C_{org}$, $\delta^{34}S_{CAS}$, $\delta^{34}S_{pyr}$ and $\delta^{18}O_{CAS}$ data for reconstructing the potential controls on these proxies during a period of rapid environmental change (Munnecke et al., 2010,

2003). The Baltoscandian Basin preserves an abundance of relatively continuous outcrop and drill core sections spanning the late Ordovician through Silurian, providing a platform to assess the causes and consequences of some of the earliest extinction events in the Phanerozoic. One such extinction event, known as the Ireviken bioevent (IBE; Calner, 2008; Jeppsson, 1997; Munnecke et al., 2003; Tonarová et al., 2014) occurs at the Llandovery-Wenlock boundary, associated with a globally documented carbon isotope excursion and paleoclimate perturbations (Lehnert et al., 2010; Trotter et al., 2016). Additionally, the short duration of the stages in the Silurian (e.g. Cramer et al., 2010), combined with the number of time-correlative stratigraphic sections in the Baltoscandian Basin, serves as a framework to evaluate whether the observed geochemical perturbations result from global environmental phenomena. We present new $\delta^{13}C_{carb}$, $\delta^{13}C_{org}$, $\delta^{34}S_{CAS}$, $\delta^{34}S_{pyr}$ and $\delta^{18}O_{CAS}$ data from the Silurian strata in the upper 112 m of the Paatsalu drill core, Estonia. This interval is temporally correlative with strata in the Viki core, Estonia (Richardson et al., 2019a), and in Gotland, Sweden (Rose et al., 2019), which together provide a basin-wide transect of early Silurian sedimentary strata.

2.0 Geological Setting

The studied Paatsalu drill core from western Estonia (Fig. 1; 58°5' N 23°7'E) spans from the mid-Llandovery to the mid-Wenlock (ca 440 to 432 Ma). The section represents the northern margin of the Baltoscandian Basin, an early Paleozoic epicontinental sea on Baltica and then Laurussia (Baarli et al., 2003; Cocks and Torsvik, 2005; Nestor and Einasto, 1997). During the early Silurian, the region was located at tropical southern latitudes (Torsvik and Cocks, 2013). Various warm-water carbonates and marly deposits accumulated in the shallow part of the basin, such as in central Estonia. Deeper shelf facies, characterized by the deposition of organic-rich muds, were located

134 towards the south and west from the study site (Fig. 1; Nestor & Einasto, 1997; Baarli et al., 2003).
135 The stratigraphic framework of the Silurian of the Paatsalu core is based largely on chitinozoan
136 and conodont biostratigraphy (Hints et al., 2006; Rubel et al., 2007) and K-bentonites (Kiipli et
137 al., 2006, 2008). Additionally, carbon isotope chemostratigraphy can be applied and numerous
138 reference sections from the region can be used for comparison (Kaljo and Martma, 2006, 2000).
139 Five formations are identified through this interval in the Paatsalu drill core: the Nurmekund,
140 Rumba, Velise, Jaani and Muhu formations.

141 The lowermost Nurmekund Formation (111.8 m depth), which correlates to the late-
142 Rhuddanian and Aeronian (Kaljo and Martma, 2000), consists of interbedded carbonate mudstone
143 and grainstone with varying abundances of bioclastic material deposited within lagoonal
144 (mudstone) and shoreline (grainstone) environments. The base of the Rumba Formation (102–83
145 m) is marked by a 2-m-thick, sharp-based, low-angle cross-bedded grainstone overlain by
146 interbedded wackestones and packstones with echinoderms, brachiopods and bryozoans, with a
147 small abundance of interbedded mudstone. These facies indicate deposition within inner-shelf, reef
148 and shoal settings. A 20-cm-thick bentonite bed at 88 m depth is correlative with one at 185.1 m
149 depth in the Viki core (Kiipli et al., 2006). The overlying Velise Formation (83–70 m depth) is
150 composed of grey-green siliciclastic mudstone and marlstone with abundant pyrite in the form of
151 small aggregates, large euhedral crystals and pyritized burrows and echinoderm fragments; these
152 facies represent a mid- to outer-shelf setting. Partial dolomitization of the carbonates begins in the
153 middle of the Velise Formation through to the top of the core. An erosive-based 1-m-thick oolitic
154 packstone at 70.5 m marks the base of the Jaani Formation (70–34 m depth), defining a sequence
155 boundary placing inner-shelf facies (the oolite) on top of mid-outer shelf marlstones (Velise
156 Formation). Above this, the Jaani Formation consists of dolomitized grey-green mud-marlstones

like those in the Velise Formation. Macroscopic pyrite is visible within the first meter of the marlstone, but size and abundance decrease upwards. The marlstone grades into bioclastic, nodular micritic limestone, reflecting a progressive shallowing into mid-shelf settings. The Muhu Formation (34 m depth to top of the core) consists of interbedded bioclastic (echinoderms, brachiopods, bryozoans) wackestone and packstone in the lower 11 m, with an increasing abundance of mud drapes upward into thinly interbedded dolomitic arenite with dolomitized mudstone and wackestone at the top of the core. Overall, the succession records two large-scale depositional cycles. The Nurmekund formation represents the upper part of the "Early-Middle Llandovery macrocycle" (Nestor & Einasto, 1997); it is followed by a regional hiatus and denudation during the late Aeronian. The "Late Llandovery - Middle Wenlock macrocycle" is represented by a full transgressive-regressive cycle in the Paatsalu core: a gradual deepening to inner-mid shelf settings (Rumba Formation) and even deeper mid-outer shelf facies (Velise Formation) during the Telychian; then a sequence boundary that coincides with a gap (Männik et al., 2014) and marks a return to inner-mid shelf settings (oolite at the base of the Jaani Formation) with a subsequent flooding surface to outer-shelf facies (Jaani Formation) and then shallowing into peritidal environments (Muhu Formation). As a result of the early-mid Wenlock regression the basin transformed into a more restricted gulf-like pericratonic sea (Nestor & Einasto, 1997).

3.0 Methods

The Paatsalu drill core material is housed at the Särghaua core repository, Tallinn University of Technology (https://geocollections.info/drillcore/128). A total of 62 samples from the Paatsalu core were collected, cut, crushed and powdered in a Spex 8515 Shatterbox. Homogenized powders were divided for each type of analysis. Carbon and sulfur isotope analyses, together with elemental

abundance analyses, were carried out at Washington University in St. Louis, USA. Analyses for oxygen isotopes of CAS were performed in the analytical facilities at Indiana University-Purdue University Indianapolis, USA.

For carbonate carbon and carbonate oxygen isotope analyses, ~100 µg of sample powder was dissolved in 100% phosphoric acid (H_3PO_4) for at least 4 hours at 70°C (accounting for differences in acid digestion of calcite-dolomite mixtures; Xi Liu et al., 2019). Sample vials were flushed with He and the evolved CO_2 was measured on a Thermo Finnigan Gasbench II coupled to a Delta V Advantage Isotope Ratio Mass Spectrometer. Organic carbon isotope analyses were performed on the organic residue left after decarbonating 4–5 g of sample powder with 6M HCl. Acidifications were left for up to 20 minutes and were repeated until there was no visible reaction when HCl was added. Insoluble residues were analyzed for organic carbon isotope composition on a Flash 2000 Organic Elemental Analyzer coupled via a ConFlo IV to a Delta V Plus Isotope Ratio Mass Spectrometer. Carbon and oxygen isotopes are expressed in standard delta notation ($\delta^{13}C$, $\delta^{18}O$) in permil (‰) relative to the Vienna Pee Dee Belemnite (VPDB) standard with 1 σ error on $\delta^{13}C_{carb}$, $\delta^{18}O_{carb}$ and $\delta^{13}C_{org}$ of 0.15‰ based on standard and replicate samples.

Preparation of samples for analysis of sulfur and oxygen isotopic ratios in CAS and for analysis of sulfur isotopic ratios of pyrite followed Richardson et al. (2019a). Sample powder (30–50 g) was soaked in a 10% brine (NaCl) solution for 30 minutes and then decanted. This step aimed to remove any free sulfur species that might be adsorbed onto the carbonate. After a total of three brine rinses, the supernatant was checked for sulfate by adding 1 ml of saturated $BaCl_2$ solution and additional brine rinses were performed if any precipitate formed in the supernatant. This was followed by 3 rinses with deionized H_2O. Samples were acidified with 6M HCl and stirred for up to 3 hours (or until there was no visible reaction) to release CAS. The acidic supernatant was

filtered and reacted with an excess of $BaCl_2$ to precipitate $BaSO_4$ which was rinsed, weighed and dried for analyses. To extract pyrite as chromium-reducible sulfur (Canfield et al., 1986), insoluble residues from the CAS extraction were reacted with a 6M HCl and 2M chromium (II) chloride solution under constant N_2 gas and were left stirring for 4 hours just below the boiling point. The evolved gas from the sample reaction was passed through a water trap and bubbled into a test tube containing silver nitrate solution in deionized H_2O in order to precipitate silver sulfide.

Sulfur isotope analyses were performed by combining ~350 μg of silver sulfide or barium sulfate with 1–3 mg of vanadium pentoxide and converted to SO_2 using a Costech ECS 4010 elemental analyzer coupled to a Thermo Finnigan Delta V Plus mass spectrometer. Separate aliquots of 150 μg barium sulfate (from both the Paatsalu and Viki core) were combined with an equal amount of graphite in a silver capsule then loaded into a nitrogen-purged Costech Zero-blank autosampler and analyzed for oxygen isotopes by pyrolysis (at 1450ºC) using a Thermo TC/EA coupled to a Thermo Delta V Plus mass spectrometer. Sulfur isotope values are expressed in standard delta notation ($\delta^{34}S$) in permil (‰) as a deviation from the Vienna Canyon Diablo Troilite (VCDT) standard and have a 1σ error of 0.3‰ and 0.2‰ for $\delta^{34}S_{CAS}$ and $\delta^{34}S_{pyr}$ respectively. The oxygen isotope composition of sulfate is reported in delta notation ($\delta^{18}O$) relative to Vienna Standard Mean Ocean Water (VSMOW), where the 1σ error on $\delta^{18}O_{CAS}$ is 0.2‰, based on standards and replicate samples.

Elemental abundance within the carbonate fraction of rock powders were prepared following the protocol of Husson et al., (2015). Data were collected using a PerkinElmer Optima 7300DV ICP-OES and standardized to the Sigma Multi-element Standard Solution 5. Abundances are given in ppm.

4.0 Results

4.1 Carbon Isotopes

The strata from the Paatsalu core preserve a smoothly varying $\delta^{13}C_{carb}$ record (Fig. 2). In the Nurmekund Formation, $\delta^{13}C_{carb}$ increases from 0‰ to 1.3‰ between 111.8 and 108.5 m depth before declining to -1.3‰ at 98.2 m depth in the lower Rumba Formation ('Rumba low'; Kaljo and Martma, 2000). Values increase to 0.4‰ at 86.2 m depth and jump to 2‰ at 83.4 m depth (over a discontinuity in sampling) near the top of the Rumba Formation and remain near 2‰ through the Velise Formation. Between 70 and 66 m depth, in the oolitic packstone at the base of the Jaani Formation, $\delta^{13}C_{carb}$ values increase to 4‰, reaching a maximum of 4.8‰ at 51 m depth and from there decrease steadily through the Muhu Formation to around -0.4‰ at the top of the core. The positive $\delta^{13}C_{carb}$ excursion to 4.8‰ is approximately time-correlative to the IBE recorded in numerous sections worldwide (Hints et al., 2006; Munnecke et al., 2003; Richardson et al., 2019a; Rose et al., 2019).

The base of the Nurmekund Formation is marked by $\delta^{13}C_{org}$ values of -29‰ that decrease to -31.2‰ in the lower part of the formation (Fig. 2). $\delta^{13}C_{org}$ then increases through the Rumba and Velise formations to -27.2‰ at 70 m depth and continues to increase to -24.7‰ at 68.6 m depth across the base of the Jaani Formation. Above this, there is a small decline to -26.9‰ at 38 m depth, but values increase to -25.7‰ at the top of the Formation. Notably, from c. 60 to 35 m depth $\delta^{13}C_{org}$ and $\delta^{13}C_{carb}$ show opposite trends. From 36 to 16.5 m depths $\delta^{13}C_{org}$ varies, between -26‰ and -24‰ before decreasing to -30‰ toward the top of the core.

4.2 Sulfur Isotopes

The Paatsalu $\delta^{34}S_{CAS}$ data have typical sample-to-sample variability of 1–4‰ and maximal sample-to-sample variability of 7–10‰ (Fig. 2; Table 1). The lowermost samples in the Nurmekund Formation decrease from 33‰ to 23.4‰ into the basal Rumba Formation. Values become more variable, ranging between 29.7‰ and 17.5‰, through to the top of the Rumba Formation at 84.3 m depth. In the Velise Formation, $\delta^{34}S_{CAS}$ values are more positive and less variable between 25.4‰ and 32‰. In the Jaani Formation, $\delta^{34}S_{CAS}$ values are tightly clustered around 27.5‰ (except one sample, 15‰, at 67.2 m depth) up to 46.2 m depth. Above this, values decrease into the Muhu Formation, reaching 15.6‰ at 20 m depth. From 20 m depth to the top of the core, $\delta^{34}S_{CAS}$ values vary between 3.3‰ and 14‰ to the top of the core. Overall, three main trends are observed: (i) variable $\delta^{34}S_{CAS}$ (sample-to-sample variability as much as 5.5‰) in the Nurmekund and Rumba formations; (ii) relatively invariant $\delta^{34}S_{CAS}$ between 25 and 30‰ in the Velise and Jaani formations; and (iii) declining $\delta^{34}S_{CAS}$ in the Muhu Formation, becoming increasingly variable toward the top of the core.

Sulfur isotope values in pyrite range from 1‰ to 15.4‰ in the lower 10 m of the studied section (Fig. 2; Table 1). Above 102.5 m depth, $\delta^{34}S_{pyr}$ decreases from 10.9‰ to -21.8‰ over 4 m. Between 98.2 m and 80.3 m depth (the Rumba Formation), $\delta^{34}S_{pyr}$ varies between -20‰ and -30‰ with one outlier (2.8‰) at 83.4 m depth. At 78 m, $\delta^{34}S_{pyr}$ increases to 4.6‰ and continues to increase through the Velise Formation up to 15.4‰, except for one sample (-32.3‰) at 74.24 m. At the base of the Jaani Formation values decrease to -14.3‰ and continue to decrease to -21.1‰ at 62.9 m depth. Above that, $\delta^{34}S_{pyr}$ increases to c. -2‰ at 35 m depth, stabilizes around -9‰ from 32.5 to 16.5 m depth and then decreases to -14.5‰ to the top of the core. In summary, the Nurmekund and Velise formations have highly variable $\delta^{34}S_{pyr}$ values, while the Jaani and Muhu

Formations exhibit intermediate and moderately variable $\delta^{34}S_{pyr}$ (with increasing variability in $\delta^{34}S_{pyr}$ up-section), and the Rumba Formation has the least $\delta^{34}S_{pyr}$ variability.

Table 1. Sulfur isotope variability for the Paatsalu core

Formation (n = samples)	Facies	average $\delta^{34}S_{CAS}$	avg sample-to-sample $\delta^{34}S_{CAS}$ difference	average $\delta^{34}S_{pyr}$	avg sample-to-sample $\delta^{34}S_{pyr}$ difference
Nurmekund (4)	shoreline-lagoon	28.9	3.2	8.5	8.9
Rumba (14)	inner-mid shelf	24.8	3.3	-19.9	4.5
Velise (9)	mid-outer shelf	29.3	2.6	-7.6	16.4 (8.3)
Jaani (30)	outer shelf	27.2	2.4	-9.6	7.0 (4.2)
Muhu (12)	shoreline	14.5	5.1	-9.8	5.7

4.3 Oxygen Isotopes

The $\delta^{18}O_{carb}$ values in the Nurmekund Formation decrease from -5.2‰ to -6.7‰ at 102.6 m. In the Rumba and lower Velise formations, values remain around -6‰ to ~71.5 m depth and become increasingly variable up to 59 m depth in the lower Jaani Formation. Values converge around -6‰ at 39.3 m depth and variability decreases. There is a step increase in $\delta^{18}O_{carb}$ values from -5.5‰ to -2‰ around 39 m depth, with values stabilizing around -4‰ through to the top of the core. In general, $\delta^{18}O_{carb}$ values are relatively invariant, between -5‰ and -7‰, in the Nurmekund Formation through the base of the Muhu Formation (111.8 to 39.3 m depth; Fig. 2). $\delta^{18}O_{carb}$ values are higher and more variable between -2‰ and -4.5‰ from 39 m to the top of the core.

The oxygen isotope values of CAS have similar stratigraphic variability and trends as $\delta^{34}S_{CAS}$ (Fig. 2). At the base of the Paatsalu section, $\delta^{18}O_{CAS}$ is 12.4‰ and decreases to 10.6‰ at 105.3 m depth. Values increase variably from 10‰ to 15.6‰ at the top of the Velise Formation at

71.5 m depth. In the Jaani Formation (67.2 m depth), $\delta^{18}O_{CAS}$ decreases to 8.3‰ before increasing to 14.5‰ at 63 m depth and then remains relatively invariant. From 42 to 26.9 m depth, $\delta^{18}O_{CAS}$ becomes increasingly variable (between 11.5‰ and 15‰ with one outlier of 20.3‰ at 36 m depth), and then decreases through the Muhu Formation, reaching the lowest $\delta^{18}O_{CAS}$ value in the core (-1.2‰ at 9.6 m depth).

To complement these data from the Paatsalu core, we also present new $\delta^{18}O_{CAS}$ data from the previously studied Viki core (Fig. 3). The base of the Viki core begins in the Varbola Formation (see Richardson et al., 2019a) at 240.6 m depth with $\delta^{18}O_{CAS}$ of 17.9‰, which decreases throughout the Varbola Formation to approximately 15‰ at 228.5 m depth. $\delta^{18}O_{CAS}$ is variable between 11.5 and 17.4‰ through the upper Varbola and lower Nurmekund formations. At 208.4 m, $\delta^{18}O_{CAS}$ increases from 12.4 to 16.5‰ at 180 m depth in the lowermost Velise Formation. From 168.3 – 107.4 m depth, values are variable around 15‰ throughout the Velise and lower Jaani formations. Above this, $\delta^{18}O_{CAS}$ increases to 20‰ at 97.7 m depth before returning to 15‰ at 87.6 m depth in the upper Jaani Formation. From 87.6 m to the top of the section, $\delta^{18}O_{CAS}$ values increase to 17.4‰.

5.0 Discussion

Carbon, sulfur and oxygen isotopic ratios in carbonate successions have been used to track the operation and evolution of global biogeochemical cycles through geologic time (Canfield, 2001; Kump and Arthur, 1999). However, frequency, magnitude and duration of isotopic changes can also result from basin-specific processes, depositional controls, diagenesis, or combinations of these processes. Therefore, the nature of isotope excursions must be independently assessed in any given succession. Within the Paatsalu core, carbon isotopic ratios in carbonate and organic matter

generally co-vary, whereas sulfur isotopic records of $\delta^{34}S_{CAS}$ and $\delta^{34}S_{pyr}$ do not. Additionally, the variability in $\delta^{34}S_{CAS}$, $\delta^{18}O_{CAS}$ and $\delta^{34}S_{pyr}$ (Table 1) commonly occurs too rapidly (with respect to the residence time of seawater sulfate) for this variability to reflect global perturbations to the seawater sulfate reservoir via canonical, global-scale mechanisms. Fluid inclusion data from the Silurian shows seawater sulfate concentrations from 5-12 mM (Lowenstein et al., 2003), approximately 17-43% of the modern ocean value. The residence time of a reservoir is the ratio of the size of the reservoir to the input or output flux; estimates for modern seawater sulfate residence times range from 13-20 Ma (Canfield 2004; Bottrell and Newton, 2006). Based on conodont biostratigraphy, this 112 m section of the Paatsalu core records < 15 Myr (Figs. 2 and 3), and the carbon isotope excursion (coincident with the IBE) lasts ~1 Myr (Cramer et al., 2011). In addition, the size of the modern ocean sulfate reservoir buffers $\delta^{34}S_{SO4}$ to a maximum rate of change of 0.5‰ per Myr (Kah et al., 2004). Here, an average rate of change for $\delta^{34}S_{CAS}$ of 1.3‰ per Myr would require seawater sulfate concentrations to be < 4.5 mM for this rate of change to be consistent with the size of the expected marine sulfate reservoir (Kah et al., 2004). Thus, marine sulfate should have relatively invariant $\delta^{34}S_{SO4}$ and $\delta^{18}O_{SO4}$ values over the timescale of the individual formations recovered in the Paatsalu core. As noted above, variability in $\delta^{34}S_{CAS}$, $\delta^{18}O_{CAS}$ and $\delta^{34}S_{pyr}$ show high sample-to-sample variability, which we consider to be far too rapid to reflect worldwide perturbations to the global sulfur cycle.

5.1 Diagenesis

For reliable interpretation of the evolution of local or global biogeochemical cycles as recorded by geochemical signatures, it is essential to assess diagenetic alteration of carbonate proxies by fluid migration, carbonate recrystallization, or dolomitization during early or late marine diagenesis, or

by non-marine fluids during burial or meteoric diagenesis (e.g. Banner and Hanson, 1990; Halverson et al., 2007; Marenco et al., 2008b). Carbonate diagenesis is complex and can impact mineralogy, lithofacies and different portions of carbonate platforms heterogeneously. Consequently, there are a number screening tools used to interpret the extent of diagenetic alteration of the geochemical signals that are of interest to our understanding of past Earth environments (Swart, 2015). To assess the *most likely* alteration mechanisms influencing sulfur isotope signals (values and variability) and to determine the *least altered* $\delta^{34}S_{CAS}$ values we used: (1) elemental analyses and isotope relationships as a coarse indicator for determining the type of fluid-rock interaction; (2) $\delta^{34}S_{CAS}$ and abundance relationships to assess direct influences on $\delta^{34}S_{CAS}$; (3) evaluation of geochemical data within a lithologic context; and (4) assessment of $\delta^{34}S_{CAS}$ and $\delta^{18}O_{CAS}$ relationships to understand inherent early marine diagenetic processes.

5.1.1 Post-depositional fluid-rock interactions

Common indicators of diagenesis, such as Sr abundance and correlations between Mn vs. Sr, Fe vs. Sr and $\delta^{13}C_{carb}$ vs. $\delta^{18}O_{carb}$, are generally used to screen samples for evidence of meteoric, burial, brine and marine diagenesis (Banner and Hanson, 1990; Bartley et al., 2001; Erhardt et al., 2020; Halverson et al., 2007; Turchyn et al., 2009). Sr abundance is considered an approximate indication of the degree of carbonate recrystallization, as most fluids distinct from seawater will remove Sr from carbonate minerals with progressive recrystallization. In this study all samples have Sr abundance < 200 ppm (Fig. 4) which is much lower than typical 'primary' carbonate (often > 1000 ppm). Thus the entire succession has likely experienced some degree of alteration and we do not consider stratigraphic changes in Sr abundance a clear indicator for the type of fluid interaction in these samples (Ahm et al., 2018; Halverson et al., 2007).

Although Mn, Sr and Fe relationships were initially understood to reflect varying degrees of meteoric diagenesis (Brand and Veizer, 1980), Mn, Sr and Fe correlations can also help evaluate the degree of fluid interactions under anoxic conditions (e.g. Turchyn et al., 2009). Our data show increases in Mn and Fe with concurrent decreases in Sr, possibly indicating meteoric diagenesis or progressive carbonate recrystallization under anoxic conditions (Figs 4A-B). Lime mudstone, wackestone, and packstone facies from the Nurmekund and Rumba Formations have the highest Sr and lowest Mn and Fe abundances, suggesting that these facies are the least diagenetically altered, though not necessarily primary (Fig. 4A). In contrast, $\delta^{13}C_{carb}$ vs. $\delta^{18}O_{carb}$ do not covary (Fig. 4C), even those samples from outside the positive $\delta^{13}C_{carb}$ excursion, in a manner consistent with alteration by meteoric or burial (brine) fluids (Banner and Hanson, 1990), where meteoric fluids are depleted in both ^{13}C and ^{18}O while brine fluids are commonly depleted in ^{18}O relative to seawater (Swart, 2015). In addition, the small offset between $\delta^{18}O_{carb}$ presented here and $\delta^{18}O_{carb}$ values from similarly aged, well-preserved brachiopods (-4.5 to -5.5‰; Azmy et al., 1998), suggests that $\delta^{18}O_{carb}$ in the Paatsalu section has been affected by seawater-like diagenetic fluids, perhaps under anoxic conditions. Despite this, we find no correlation between $\delta^{18}O_{carb}$ and any other geochemical parameter measured. Together, this indicates correlations between Mn, Fe and Sr are most likely due to fluid interactions under anoxic conditions.

To assess alteration associated with dolomitization, lithology-specific $\delta^{34}S_{CAS}$ is plotted against Mg/Ca ratio (Fig. 5A) (Marenco et al., 2008b). Samples with Mg/Ca ratio < 0.125 have $\delta^{34}S_{CAS}$ values between 21‰ and 33‰, which is not uncommon for unaltered marine carbonates of this age (Present et al., 2020) and is similar to those in the nearby Viki core (Richardson et al., 2019a). At higher Mg/Ca ratios (> 0.35), $\delta^{34}S_{CAS}$ values span the entire range observed in the Paatsalu core. The large range of $\delta^{34}S_{CAS}$ in the dolomitized samples could indicate distinct

dolomitizing processes that give rise to both increased and decreased $\delta^{34}S_{CAS}$ values. Partial dolomitization is present from 75 m to the top of the Paatsalu core (from the top of the Velise through the Muhu Formation). The $\delta^{34}S_{CAS}$ of dolomitized samples from the upper Velise and Jaani Formation are relatively stable (varying between ~ 25‰ and 30‰) and are similar to the $\delta^{34}S_{CAS}$ values from unaltered marlstone of the lower Velise Formation (Fig. 5). This implies that the dolomitizing fluids did not overprint $\delta^{34}S_{CAS}$ from the upper Velise and Jaani Formation, such that the composition of the dolomitizing fluid was not appreciably offset from seawater. Comparatively, the Muhu Formation has the least variable and highest Mg/Ca ratios and also records the lowest $\delta^{34}S_{CAS}$ values (3-25‰). In this case, the composition of the dolomitizing fluid progressively evolved with sulfate sourced from sulfide oxidation, decreasing $\delta^{34}S_{CAS}$ values in the recrystallizing carbonate. The dolomitizing fluid was the most evolved during dolomitization of the uppermost Muhu Formation, where $\delta^{34}S_{CAS}$ values are particularly low (3-15‰). It has been shown that enhanced evaporation and MSR can encourage dolomitization (Baldermann et al., 2015; Fichtner et al., 2017), and such dolomitization has been shown to incorporate isotopically light ^{34}S-sulfate, particularly in near shore environments (e.g. Fichtner et al., 2017; Marenco et al., 2008b; Present et al., 2015). This process may have had an additional impact on the $\delta^{34}S_{CAS}$ values of the upper Muhu Formation. The lower but more variable $\delta^{34}S_{CAS}$ values with elevated Mg/Ca from the higher energy peritidal environments is the inverse facies relationship observed in Present et al., (2019). This suggests that dolomitization influences more local controls on $\delta^{34}S_{CAS}$ evolution in this basin and highlights the importance of assessing which facies best preserve $\delta^{34}S_{CAS}$ in a given carbonate succession. Overall this information suggests that late-stage post-depositional fluids (meteoric or burial) did not reset the isotope proxies throughout the Paatsalu core, and that variability in the isotopic compositions must result from smaller scale, more localized processes.

400

401 *5.1.2 Sulfide oxidation: decreased $\delta^{34}S_{CAS}$ and $\delta^{18}O_{CAS}$*

402 Early marine diagenetic processes can generate correlated local increases and decreases in $\delta^{34}S_{SO4}$
403 and $\delta^{18}O_{SO4}$ of porewater, which can then be retained in the (re)precipitating carbonate $\delta^{34}S_{CAS}$
404 and $\delta^{18}O_{CAS}$ values (e.g. Goldberg et al., 2005; Rennie and Turchyn, 2014). Sulfide (and pyrite) is
405 ^{34}S-depleted relative to sulfate due to MSR, and when it is oxidized the product sulfate will inherit
406 these lower $\delta^{34}S$ values. The same sulfide that is oxidized will incorporate oxygen from the
407 ambient fluid which lowers the resultant $\delta^{18}O_{SO4}$ (Goldberg et al., 2005; Newton et al., 2004).
408 Negative correlations in plots of $\delta^{34}S_{CAS}$ vs. CAS and/or pyrite abundance can indicate the
409 influence of pyrite oxidation, particularly during laboratory extractions (Marenco et al., 2008a). In
410 the Paatsalu data, there are no general correlations between $\delta^{34}S_{CAS}$ and CAS or pyrite abundance
411 (Fig. 5B and C) meaning that influence of pyrite oxidation during laboratory extraction on sulfur,
412 and therefore oxygen isotopes, in CAS can be excluded. However, samples with the lowest $\delta^{34}S_{CAS}$
413 values (< 15‰; much lower than what is observed during laboratory extraction, Marenco et al.,
414 2008a) also contain the greatest, yet also most variable, abundance of CAS (Fig. 5B). This
415 correlation is not systematic but most likely reflects variable sulfide/pyrite oxidation and
416 subsequent incorporation of sulfate as CAS under oxic conditions, a process known to impact
417 modern sediments (Percak-Dennett et al., 2017). The correlation of anomalously low $\delta^{34}S_{CAS}$
418 values (3-15‰), compared to Ordovician-Silurian seawater from evaporite minerals (25.5‰;
419 Kampschulte and Strauss, 2004), with similarly low $\delta^{18}O_{CAS}$ values (-1.7-10‰; Fig. 6A) is further
420 evidence to support that these samples have been the most influenced by sulfide oxidation (e.g.
421 Goldberg et al., 2005). Samples with $\delta^{34}S_{CAS}$ values 20-25‰ may also have incorporated sulfur
422 isotope values from locally oxidized sulfide, although to a lesser extent.

Depositional environmental conditions give rise to localized decreases in $\delta^{34}S$ and $\delta^{18}O$ of ambient seawater (porewater) sulfate. In shallow water environments, the frequency of sedimentary reworking increases (e.g. by bioturbation, tides and storms), resulting in punctuated oxidation of the pore fluid as well as frequent exposure to air. This is likely to have influenced samples with moderately low $\delta^{34}S_{CAS}$ (20-25‰) which are predominantly observed within wackestone and packstone facies (Fig. 5D). Additionally, tidal environments are influenced by continental freshwater, where weathering of pyrite on land causes low $\delta^{34}S$ values of riverine sulfate. However, freshwater typically has lower concentrations of sulfate compared to seawater and would result in a decrease of CAS abundance (Gill et al., 2008). Although continental-derived fluids may interact with carbonates at any time, we suspect that the influence of continental fluids is minor and may only be preserved in a small number of samples from the Muhu Formation (Fig. 2 at 4.5 and 22.7 m) with those samples containing low CAS abundance, low Sr, and high Fe and Mn. Although these geochemical parameters are consistent with possible meteoric influence, $\delta^{18}O_{Carb}$ values do not support a clear meteoric influence on these samples. Thus an alternate explanation for very low $\delta^{34}S_{CAS}$ values (down to 3‰) is required, such as dolomitization coupled with sulfide oxidation as discussed above.

5.1.3 Microbial Sulfate Reduction: increased $\delta^{34}S_{CAS}$ and $\delta^{18}O_{CAS}$

Microbial sulfate reduction, considered an early marine diagenetic process, results in correlated increases in sulfur and oxygen isotopic compositions in residual porewater sulfate, particularly under closed system conditions where the rate of sulfate consumption in porewater is greater than the rate sulfate is replenished by the diffusion of seawater (Goldberg et al., 2005). MSR increases alkalinity, promoting carbonate precipitation in pore spaces (Baumgartner et al., 2006; Berner et

al., 1970). Thus, newly precipitating and/or recrystallizing carbonate has the potential to incorporate these evolved porewater sulfate signals into CAS, elevating $\delta^{34}S_{CAS}$ and $\delta^{18}O_{CAS}$ values (Antler et al., 2013; Goldberg et al., 2005; Rennie and Turchyn, 2014).

In addition to porewater sulfate isotopes evolving with increasing depth beneath the sediment surface, platform-scale progressive evolution of pore fluids can also occur, associated with basinward migration of platform-top brines (Al-Helal et al., 2012) or shoreward migration of seawater (e.g. Jones et al., 2019). These processes would also result in progressively increasing porewater $\delta^{34}S_{SO4}$ and $\delta^{18}O_{SO4}$ along the direction of the flow path (vertical and lateral), as continued MSR will progressively remove ^{32}S. Evidence for platform-scale evolution of pore-fluids is observed in the stratal geometry of the dolomite between the Paatsalu and Viki cores; all samples from the Jaani and Muhu Formations show partial dolomitization in the Paatsalu core, yet only samples from the upper Jaani and lower Jaagarahu Formation (time correlative to the Muhu Formation) in the Viki core are partially dolomitized (Richardson et al., 2019a). In this case, the chemical evolution of local pore-fluids during basinward migration from the shallow-water facies (e.g. upper Jaani Formation, Viki core), would result in increased $\delta^{34}S_{SO4}$ in deeper water facies (e.g. Jaani Formation, Paatsalu core). We speculate that the evolution of $\delta^{34}S_{SO4}$ and $\delta^{18}O_{SO4}$ in pore spaces in shallow-water environments (due to MSR), and the migration of these fluids to deeper environments might best explain the increase in $\delta^{34}S_{CAS}$ values (~30‰) in the middle of the deep-water facies of the Jaani Formation in the Paatsalu core. This hypothesized migration of pore fluids associated with dolomitizing fluids may be recorded in other isotope systems such as $\delta^{44}Ca$ and $\delta^{26}Mg$, where paired $\delta^{44}Ca$ and $\delta^{26}Mg$ data could differentiate between fluid- and sediment-buffered conditions during dolomitization. An examination of cross-plots of $\delta^{18}O_{CAS}$ vs. $\delta^{34}S_{CAS}$ can help assess closed-system behavior associated with parallel positive shifts in oxygen

and sulfur isotopic compositions (Fig. 6). Values of $\delta^{34}S_{CAS}$ and $\delta^{18}O_{CAS}$ are positively correlated (Fig. 6A), even when removing the subset of samples most influenced by sulfide oxidation (Fig. 6B). Similar correlations of $\delta^{34}S_{CAS}$ and $\delta^{18}O_{CAS}$ relationships are observed in the Viki core (Fig. 7A and 7B). Wackestone, packstone, and partially dolomitic marlstone facies show the strongest $\delta^{34}S_{CAS}$-$\delta^{18}O_{CAS}$ correlation (Fig. 6C). Additionally, $\delta^{34}S_{CAS}$ shows greater variability in wackestone and packstone facies compared to the dolomitic marlstone (Fig. 5D and 6C), potentially attributable to the increased, yet pulsed, nature of shallow-water sedimentation (e.g. Aller et al., 2004; Aller et al., 2010; Richardson et al., 2019a).

In the absence of any correlations between late-stage diagenetic indicators (e.g. $\delta^{13}C_{carb}$ vs. $\delta^{18}O_{carb}$, see *5.1.1*), Mn/Sr can be used as an indication of precipitation or recrystallization in anoxic pore fluid during early marine diagenesis (e.g. Turchyn et al., 2009b). This tool is based on low Mn/Sr ratios in modern seawater (i.e. $< 4x10^{-7}$, see Chester, 1990) and high Mn/Sr in evolved waters (Brand and Veizer, 1980), suggesting that anoxic pore fluids that evolved from seawater will concentrate Mn. As such, Mn/Sr ratios are used as a screening tool, typically assigning a threshold above which samples are excluded from primary geochemical interpretation of $^{87}Sr/^{86}Sr$, $\delta^{13}C$ and $\delta^{34}S_{SO4}$ (Bartley et al., 2001; Fölling and Frimmel, 2002; Gómez Peral et al., 2007; Tostevin et al., 2017; Turchyn et al., 2009). However, Mn/Sr values < 1 have been found in modern carbonates substantially affected by early marine diagenesis (Higgins et al., 2018), calling into question the usefulness of a Mn/Sr threshold in ancient carbonates that have likely experienced more diagenesis than modern carbonate platforms. We use Mn/Sr as an additional assessment of $\delta^{34}S_{CAS}$ values that have been most impacted by MSR (i.e. carbonate precipitating or recrystallizing in anoxic conditions associated with sulfate reduction). In this context, a majority of Paatsalu samples have a recrystallized signature (Fig. 6D). However, these samples fall into two

492 groups, samples with Mn/Sr < 3.5 from the shallow-water facies in the Nurmekund and Rumba
493 Formations, and samples Mn/Sr > 3.5 from the base of the Velise to the top of the core. Based on
494 the grouping of samples, $\delta^{34}S_{CAS}$ vs. $\delta^{18}O_{CAS}$ is replotted in these groups and a positive correlation
495 between these proxies is only observed for samples with Mn/Sr > 3.5 (Fig. 6E). Similar
496 correlations are present in the Viki samples, yet with a slightly lower Mn/Sr grouping of 3. In the
497 Viki core, a majority of samples with Mn/Sr > 3 are from the Muhu and Jaani Formations, with a
498 lesser contribution from the Velise Formation (Fig. 7C and 7D). A majority of the samples with
499 Mn/Sr > 3.5 also have higher Mg/Ca ratios and are partially dolomitized, yet this is not always the
500 case, even for the Viki core. These observations suggest that the enrichment in $\delta^{34}S_{CAS}$ and $\delta^{18}O_{CAS}$
501 tracks newly precipitating carbonate or recrystallization in a marine diagenetic realm under
502 isotopically evolving anoxic pore fluids.

503 We infer that correlated increases in $\delta^{34}S_{CAS}$ and $\delta^{18}O_{CAS}$ in Paatsalu strata record evolving
504 porewater sulfate associated with varying amounts of MSR and varying rates of carbonate
505 recrystallization in the different paleoenvironments. In this framework, the most evolved
506 porewater sulfate values plot in the upper-right and the least evolved (and therefore most
507 representative of seawater $\delta^{34}S_{SO4}$ and $\delta^{18}O_{SO4}$) samples are in the bottom-left quadrant in $\delta^{34}S_{CAS}$
508 vs. $\delta^{18}O_{CAS}$ (Fig. 6B; excluding samples clearly affected by sulfide oxidation). We suggest that
509 seawater $\delta^{34}S_{SO4}$ was approximately 27-28‰ and $\delta^{18}O_{SO4}$ was 14-15‰ during deposition of
510 Paatsalu strata based on visual clustering of samples (Fig 6C) and the frequency of samples with
511 these values in the dolomitized marlstone (i.e. deep-water facies). This deep-water facies likely
512 formed in more open connectivity with seawater with respect to the shallow-water settings. This
513 $\delta^{34}S_{SO4}$ range agrees with time-equivalent $\delta^{34}S_{CAS}$ values from brachiopods from Gotland (Present,
514 2018) although is somewhat heavier than time-equivalent evaporite data (Kampschulte and

515 Strauss, 2004). Progressive MSR and sulfide oxidation can increase and decrease porewater
516 $\delta^{34}S_{SO4}$ and $\delta^{18}O_{SO4}$, respectively, relative to coeval seawater (Goldberg et al., 2005). We observe
517 here that these signals can be preserved in recrystallized carbonates as CAS. This observation can,
518 in part, explain the elevated variability in many deep-time $\delta^{34}S_{CAS}$ records that cannot otherwise
519 be reconciled with behavior of the relatively invariant marine sulfate reservoir.
520
521 *5.1.4 Relative timing of carbonate diagenesis*
522 As discussed, many factors can contribute to the measured isotope signal in carbonate sediments.
523 Disentangling these processes can help to identify the *most primary* values in a given section. We
524 suggest the following diagenetic sequence of early marine and late marine diagenesis, followed by
525 dolomitization, for the evolution of sulfur isotope proxies in the Paatsalu core. First, early marine
526 diagenetic MSR increases pore fluid $\delta^{34}S$ values where carbonate cement and pyrite form. In
527 shallow-water environments, bioturbation, tidal activity, and wave action disturb the isotope
528 stratification in the sediment (e.g. Aller, 2004; Aller et al., 2010) by introducing seawater sulfate
529 into the sediment, and by potentially oxidizing pore water sulfide. Ultimately, this generates
530 isotopic variability between precipitating components. Proximity to the paleoshoreline (e.g.
531 interbedded arenite, Muhu Formation, Paatsalu core) influences the frequency of tidal reworking,
532 aerial exposure and interaction with continental water, which can result in localized sulfide
533 oxidation and subsequent incorporation of non-marine $\delta^{34}S_{CAS}$ values during carbonate formation
534 or recrystallization. These processes are dependent on depositional environment conditions and
535 can be considered syndepositional. Second, post-depositional marine diagenesis is common to
536 carbonate platforms, resulting in carbonate recrystallization (Christ et al., 2015). In this case,
537 platform-scale evolution of pore fluids from shallow-water environments (with distilled isotope

538 ratios) in the eastern portion of the basin migrated to deeper environments resulting in an increase
539 of $\delta^{34}S_{CAS}$ of precipitating/recrystallizing carbonate in distal settings. Dolomitizing fluids in the
540 Baltoscandian basin were associated with different styles of diagenesis and occurred
541 synchronously and/or post-dated late marine diagenetic processes. In the nearshore environments,
542 these dolomitizing fluids, with sulfate sourced in part by sulfide oxidation, may have had a greater
543 impact, decreasing $\delta^{34}S_{CAS}$ values in the newly formed dolomite (although this requires additional
544 detailed petrographic investigations to elucidate). Importantly the early marine 'syndepositional'
545 processes are inherent to most carbonate platforms throughout Earth history. Additional insight
546 into the sequence of diagenetic processes could be gained in the future through component-specific
547 (i.e. individual fossil, cement or micrite phases) isotope analyses, such as via MC-ICP-MS
548 (Johnson et al., 2020; Present et al., 2019, 2015) or SIMS (Bryant et al., 2020; Xiao et al., 2020).
549
550 *5.2 Intra-basin isotope variability*
551 *5.2.1 Carbon isotopes*
552 The existence of multiple time-equivalent chemostratigraphic profiles provides a means to assess
553 the reproducibility of data across the Baltoscandian Basin. Compared to the Viki core, the
554 chemostratigraphic record of the Paatsalu core is more complete in the lower mid-Llandovery, but
555 is condensed in the upper Llandovery to the early-Wenlock due to differences in sedimentation
556 rate and erosion (Rubel et al., 2007). The overall trends in paired $\delta^{13}C_{carb}$-$\delta^{13}C_{org}$ are consistent
557 between the two drill cores (Fig. 3) except for a slight decrease in $\delta^{13}C_{org}$ during the peak of the
558 $\delta^{13}C_{carb}$ isotope excursion associated with the IBE in the Paatsalu data. This anti-correlation in
559 carbon isotopes in the Jaani Formation is site-specific (Richardson et al., 2019a; Rose et al., 2019;
560 Young et al., 2019), reflecting an increase in the apparent biological fractionation. The magnitude
561 of the $\delta^{13}C_{carb}$ isotope excursion during the IBE is ~ 0.2‰ lower in Paatsalu compared to the Viki

562 core and they are both ~ 0.5-0.8‰ lower than the record from Gotland (Rose et al., 2019). Such
563 differences in the magnitude of carbon isotope variation between Estonia and Gotland could be
564 due to variations in the local $\delta^{13}C_{DIC}$ gradient generated by the biological pump, exporting more
565 ^{13}C-depleted carbon to deeper settings specifically at the Gotland site during the IBE, which
566 resulted in a greater increase in $\delta^{13}C_{carb}$ of the shallow water carbonates being deposited at Gotland.
567 Data across the IBE on Gotland have shown that systematic variations in $\delta^{13}C_{org}$ of different
568 organism groups may be a few per mil (Vandenbroucke et al., 2013). Thus, the extinction event
569 and associated paleoecological turnovers could have influence on average isotopic values.
570 Additionally, gradients across a carbonate platform can generate $\delta^{13}C_{carb}$ variability of up to 5‰
571 due to enhanced accumulation of ^{13}C-enriched aragonite sediment on the platform compared to
572 ^{13}C-depleted pelagic material (Geyman et al., 2021; Swart and Eberli, 2005), as well as fluid- vs.
573 sediment-buffered lithification and early marine diagenesis (Higgins et al., 2018; Jones et al.,
574 2019). Either of these processes could be the cause of the 0.2‰ difference in $\delta^{13}C_{carb}$ between the
575 Paatsalu and Viki core within the Jaani Formation.

576 Early Silurian carbon isotope records from the Baltoscandian basin record similar
577 stratigraphic signals, possibly representing a global perturbation of the carbon cycle, as evidenced
578 by the number of sections worldwide that retain coeval carbon isotopic excursions coincident with
579 the IBE (e.g. Azmy et al., 1998; Calner, 2008; Cramer and Saltzman, 2005; Lehnert et al., 2010;
580 Rose et al., 2019; Young et al., 2019). The duration of the carbon isotope excursion expressed
581 globally is < 2 Myr (Cramer et al., 2010; Nestor, 2010), which is sufficiently long for the global
582 carbon cycle to respond to a perturbation (Kump and Arthur, 1999). Previous research suggests
583 that a perturbation to the DIC reservoir (through a decrease in organic carbon burial) enhanced by
584 glacioeustatic sea level change may be the cause of the carbon isotope excursion coincident with

585 the IBE (Cramer and Saltzman, 2005; Lehnert et al., 2010; Munnecke et al., 2010; Richardson et
586 al., 2019). Local depositional effects on $\delta^{13}C$ between the sites examined are likely superimposed
587 on any global carbon isotope signal. It is important to note, however, that the effect of mineralogy
588 and fluid- versus sediment-buffered early marine diagenesis across a platform cannot be
589 discounted as a mechanism for the observed carbon isotope excursion in the Baltoscandian Basin,
590 especially given that the IBE is commonly associated with a eustatic sea level induced facies
591 change (Rose et al. 2019). Further data (e.g., $\delta^{44}Ca$ and $\delta^{26}Mg$) are required to determine if the
592 IBE $\delta^{13}C$ signal truly reflects a perturbation to the global carbon cycle or is the result of local and
593 facies-specific processes (Higgins et al., 2018; Jones et al., 2019).
594
595 *5.2.2 Sulfur isotopes*
596 No coherent basin-wide sulfur isotope excursion is observed during the IBE. The sulfur isotope
597 records are distinct in magnitude, variability and stratigraphic expression between the Paatsalu and
598 Viki cores (Fig. 3; Richardson et al. 2019a) and, importantly, a paired $\delta^{34}S_{CAS}$-$\delta^{34}S_{pyr}$ excursion
599 during the IBE on Gotland (Rose et al., 2019) is not observed in either of the Estonian sections.
600 The absence of a coherent basin-wide $\delta^{34}S_{CAS}$-$\delta^{34}S_{pyr}$ excursion indicates the sulfur isotope records
601 of these sections are not proxies for the evolution of the global or even basinal sulfate reservoir.
602 This is further evidenced by comparing Wenlock $\delta^{34}S_{CAS}$-$\delta^{34}S_{pyr}$ with sections in the USA; paired
603 $\delta^{34}S_{CAS}$-$\delta^{34}S_{pyr}$ increases throughout the early Wenlock in Nevada, yet $\delta^{34}S_{CAS}$ decreases
604 throughout the early Wenlock in Tennessee (Young et al., 2019). The sulfur isotope values
605 between Paatsalu and Viki cores and outcrop in Gotland appear to be controlled by (local)
606 depositional and early marine diagenetic processes. Although local controls on $\delta^{34}S_{pyr}$ are
607 generally well-established (Aller et al., 2010; Bryant et al., 2019; Claypool, 2004; Liu et al., 2019;

608 Pasquier et al., 2017), the effect of site-specific depositional environment and early marine
609 diagenesis on $\delta^{34}S_{CAS}$ values is less well constrained (Fike et al., 2015; Present et al., 2019; Rennie
610 and Turchyn, 2014; Richardson et al., 2019a; Rose et al., 2019), and clearly merits further study.

611 While the changes in $\delta^{34}S_{CAS}$ and $\delta^{34}S_{pyr}$ between the Estonian cores are generally not
612 coeval in timing and/or magnitude, approximately similar trends between facies packages are
613 observed between the two drill cores, albeit at slightly different times in different places on the
614 carbonate platform. The $\delta^{34}S_{CAS}$ and $\delta^{34}S_{pyr}$ values are commonly more variable in shallow-water
615 carbonate facies, likely owing to higher sedimentation rate, increased labile organic carbon
616 delivery, increased reactive iron availability, and the episodic nature of reworking events. These
617 parameters result in the development of a closed-system pore water environment and distillation
618 of isotopes during MSR, that is then variably reset by tidal/storm reworking to a more open system
619 (Aller et al., 2010; Fike et al., 2015; Richardson et al., 2019a). This process of developing more
620 closed-system conditions, punctuated by reworking events that generate more open-system
621 conditions, is a continuous cycle and results in the isotopic variability of shallow-water carbonate
622 $\delta^{34}S_{CAS}$ and $\delta^{34}S_{pyr}$. Decreased variability in $\delta^{34}S_{CAS}$ and $\delta^{34}S_{pyr}$ occurs when there is lower
623 sedimentation rate, decreased labile organic carbon delivery, and/or decreased reactive iron
624 availability, in this case occurring under higher relative sea level, e.g. in the mid-Jaani Formation,
625 the deepest setting recorded in the core (Table 1; although this trend is also seen in $\delta^{34}S_{pyr}$ of the
626 shallow-water Rumba Formation). Different depositional environments form carbonates
627 composed of varying abundances of distinct components (cement, micrite, fossils and grains). The
628 components may form above or below the sediment water interface, during early marine diagenesis
629 or any time during fluid movement, resulting in variable CAS abundance and $\delta^{34}S_{CAS}$ (Present et
630 al., 2015; Richardson et al., 2019b). For example, carbonate components precipitating in the region

631 of MSR (where concentrations of dissolved sulfate are lower) may have an overall lower CAS
632 abundance (e.g. Richardson et al., 2019b). In a plot of 1/[CAS] vs $\delta^{34}S_{CAS}$, mixing of components
633 will fall on a straight line (Fig. 5B) (Present et al., 2015). Although systematic mixing is not clear,
634 the wackestone and packstone facies (typically having the widest variety of components) indicate
635 physical mixing of CAS abundance and $\delta^{34}S_{CAS}$ of different components from a single sample.
636 This is consistent with our interpretation that shallow-water carbonates (e.g. reef facies) can be
637 unreliable proxies for global seawater $\delta^{34}S_{CAS}$ (Richardson et al., 2019a).

638 The location on the carbonate platform and facies dependence is recorded as differences in
639 the $\delta^{34}S_{CAS}$ and $\delta^{34}S_{pyr}$ values of time-correlative formations between Paatsalu and Viki sites. This
640 site-specific depositional control is attributable to the relative effect of sea-level change at each
641 location (and therefore water energy), whereby proximity to the shoreline variably drives tidal,
642 biological and sedimentation processes. For example, during sea level low-stand in the mid-
643 Llandovery, shallow-water carbonate facies (marginal marine to outer shelf) were deposited at
644 both the Paatsalu and Viki sites. However, the Paatsalu site was closer to the shoreline and the
645 shallow-water facies recorded are vertical stacks of peritidal-lagoonal sequences to inner-mid shelf
646 facies in the Nurmekund and Rumba formations, respectively. In contrast, those formations in the
647 Viki core consist of backreef to proximal shelf facies (Richardson et al., 2019a). The lower $\delta^{34}S_{CAS}$
648 values and higher sample-to-sample variability in these two formations from Paatsalu compared
649 to the Viki core reflect increased frequency of sediment reworking from wave-action and tidal
650 processes in peritidal environments. The result is a fluid-buffered system where the $\delta^{34}S$ of the
651 precipitating CAS is moderated by pore fluid $\delta^{34}S_{SO4}$ that is frequently replenished by seawater
652 (Present et al., 2019). The average $\delta^{34}S_{CAS}$ of the Nurmekund and Rumba formations in the
653 Paatsalu core is 28.9 and 24.8‰ respectively, compared to 34.38‰ and 17.3 ‰ (skewed by 4

654 samples) in the Viki core. These shallow-water facies in the Paastsalu core are closer to previous
655 estimates for $\delta^{34}S_{SO4}$ Silurian seawater (Kampschulte and Strauss, 2004; Present, 2018).
656
657 *5.2.3 Oxygen isotopes*
658 Oxygen isotopes of sulfate substantiate our conclusion that sulfur isotope signatures in the
659 Baltoscandian Basin preserve a local, early marine diagenetic signature. $\delta^{18}O_{CAS}$ values between
660 the Paatsalu and Viki cores are similar (~ 10-20‰; Fig. 3); however, there is greater variability in
661 the Paatsalu drill core. Lithology-specific $\delta^{34}S_{CAS}$-$\delta^{18}O_{CAS}$ data show similar, positive correlations
662 between facies packages in the Paatsalu and Viki drill cores (Fig. 7B and C). Mn/Sr ratios (Fig.
663 7C and D) and previous analyses support the idea that bulk isotope proxies from the Viki core have
664 not been reset by non-marine diagenesis (Richardson et al., 2019a). We suggest that the observed
665 paired $\delta^{34}S_{CAS}$-$\delta^{18}O_{CAS}$ enrichments are recording an evolving diagenetic porewater signature at
666 these locations, yet is also observed in a handful of samples from deep-water carbonate facies
667 indicative of platform-scale migration of fluids and/or carbonate recrystallization at depth within
668 the anoxic zone of the sediment.
669 The frequency and visible clustering of $\delta^{18}O_{CAS}$ values from marlstone facies (i.e. deep-
670 water facies in open connectivity with seawater) is the best assessment for most primary $\delta^{18}O_{CAS}$
671 and are comparable between the cores (14–15‰ in Paatsalu and 14-17‰ in Viki). These $\delta^{18}O_{CAS}$
672 values are similar to $\delta^{18}O_{SO4}$ of age-equivalent evaporites (Claypool et al., 1980). All other $\delta^{18}O_{CAS}$
673 values in the sections reported here, i.e. increased or decreased relative to 14-15‰, are not
674 recording changes to the global sulfur cycle. Instead, $\delta^{18}O_{CAS}$ variably records an early marine
675 diagenetic signal as a function of depositional setting, responding similarly to patterns observed in

676 $\delta^{34}S_{CAS}$. More sections should be sampled for paired $\delta^{34}S_{CAS}$-$\delta^{18}O_{CAS}$ analyses to identify the least
677 evolved values that best approximate seawater $\delta^{34}S$-$\delta^{18}O$.
678
679 **6.0 Conclusions**
680 Paired $\delta^{13}C_{carb}$-$\delta^{13}C_{org}$ data from deep-water carbonates in the Paatsalu core from the Eastern
681 portion of the Baltoscandian Basin record a positive carbon isotope excursion coincident with the
682 Ireviken Bioevent (IBE), but of slightly lower magnitude to that preserved in the equivalent
683 shallow-water formations in the western portion of the Baltoscandian basin. Variability in carbon
684 isotope composition is an expression of local depositional settings modifying a likely global
685 perturbation. In contrast, there is no basin-wide sulfur isotopic excursion observed during the IBE;
686 in the slightly more proximal setting in the east compared to the same facies packages in the west
687 basin, sulfur and oxygen isotopes record distinct stratigraphic signals, a consequence of differing
688 early marine diagenetic processes in shallow- versus deep-water settings. Paired $\delta^{34}S_{CAS}$-$\delta^{34}S_{pyr}$
689 are variable in the former and more uniform in the latter, similar to observations from paired
690 $\delta^{34}S_{CAS}$-$\delta^{34}S_{pyr}$ in the previously studied Viki core. Paired $\delta^{34}S_{CAS}$-$\delta^{18}O_{CAS}$ data preserve signatures
691 of diagenetic isotopic distillation as a result of progressive MSR in porewaters. Further, proximity
692 to paleoshorelines may also affect shallow-water $\delta^{34}S_{CAS}$, $\delta^{34}S_{pyr}$ and $\delta^{18}O_{CAS}$ values due to tidal
693 and potentially storm disruption of sediment stratification and isotope distillation. Later marine
694 diagenesis and dolomitization resulted in basinward platform-scale progressive evolution of pore
695 fluids, such that deep-water facies experienced increases in $\delta^{34}S_{CAS}$ and $\delta^{18}O_{CAS}$ values, while
696 shallow-water environments have signals associated with sulfide oxidation incorporated during
697 dolomitization. The best preserved values for $\delta^{34}S_{CAS}$ and $\delta^{18}O_{CAS}$ are near 27-28% and 14-15‰,
698 respectively, based on clustering and frequency of values in $\delta^{34}S_{CAS}$ vs $\delta^{18}O_{CAS}$ from marlstone

699 units. These values are in broad agreement with temporal time-equivalent evaporite records. Future
700 studies aiming to interpret $\delta^{34}S_{CAS}$-$\delta^{34}S_{pyr}$ data in terms of sulfur cycling should include
701 depositional context and paired $\delta^{34}S_{CAS}$-$\delta^{18}O_{CAS}$ to assess the impact of isotope distillation.
702
703 **Acknowledgements** – Acknowledgment is made to the donors of the American Chemical
704 Society Petroleum Research Fund (#57548-ND2) to D.F. for partial support of this research and
705 from the Estonian Research Council (#PUT611, #PRG836) to O.H and A.L. We thank the
706 Geological Survey of Estonia, the Department of Geology at Tallinn University of Technology,
707 and the Department of Geology at Tartu University. T. Martma is acknowledged for his help during
708 sampling of the Paatsalu section. S. Moore conducted stable isotope and ICP-OES measurements
709 at Washington University. B. Vander Pas helped prepare samples for isotope analysis at Indiana
710 University-Purdue University Indianapolis. We thank T. Present and a number of anonymous
711 reviewers for their comments that improved this manuscript.
712
713 **References**
714 Adams, D.D., Hurtgen, M.T., Sageman, B.B., 2010. Volcanic triggering of a biogeochemical
715 cascade during Oceanic Anoxic Event 2. Nat. Geosci. 3, 201–204.
716 https://doi.org/10.1038/ngeo743
717 Ahm, A.S.C., Bjerrum, C.J., Blättler, C.L., Swart, P.K., Higgins, J.A., 2018. Quantifying early
718 marine diagenesis in shallow-water carbonate sediments. Geochim. Cosmochim. Acta 236,
719 140–159. https://doi.org/10.1016/j.gca.2018.02.042
720 Al-Helal, A.B., Whitaker, F.F., Xiao, Y., 2012. Reactive transport modeling of brine reflux:
721 dolomitization, anhydrite precipitation, and porosity evolution. J. Sediment. Res. 82, 196–
722 215. https://doi.org/10.2110/jsr.2012.14
723 Aller, R.C., 2004. Conceptual models of early diagenetic processes: The muddy seafloor as an
724 unsteady, batch reactor. J. Mar. Res. 62, 815–835.
725 https://doi.org/10.1357/0022240042880837
726 Aller, R.C., Madrid, V., Chistoserdov, A., Aller, J.Y., Heilbrun, C., 2010. Unsteady diagenetic

727 processes and sulfur biogeochemistry in tropical deltaic muds: Implications for oceanic
728 isotope cycles and the sedimentary record. Geochim. Cosmochim. Acta 74, 4671–4692.
729 https://doi.org/10.1016/j.gca.2010.05.008
730 Antler, G., Turchyn, A. V., Rennie, V., Herut, B., Sivan, O., 2013. Coupled sulfur and oxygen
731 isotope insight into bacterial sulfate reduction in the natural environment. Geochim.
732 Cosmochim. Acta 118, 98–117. https://doi.org/10.1016/J.GCA.2013.05.005
733 Azmy, K., Veizer, J., Bassett, M.G., Copper, P., 1998. Oxygen and carbon isotopic composition
734 of Silurian brachiopods: Implications for coeval seawater and glaciations. Geol. Soc. Am.
735 Bull. 110, 1499. https://doi.org/10.1130/0016-7606(1998)110<1499:OACICO>2.3.CO;2
736 Baarli, B.G., Johnson, M.E., Antoshkina, A.I., 2003. Silurian Stratigraphy and Paleogeography
737 of Baltica, in: Silurian Lands and Seas. Paleogeography Outside of Laurentia. New York
738 State Museum, New York. New York State Museum Bulletin 493, 3-34.
739 Baldermann, A., Deditius, A.P., Dietzel, M., Fichtner, V., Fischer, C., Hippler, D., Leis, A.,
740 Baldermann, C., Mavromatis, V., Stickler, C.P., Strauss, H., 2015. The role of bacterial
741 sulfate reduction during dolomite precipitation: Implications from Upper Jurassic platform
742 carbonates. Chem. Geol. 412, 1–14. https://doi.org/10.1016/j.chemgeo.2015.07.020
743 Banner, J.L., Hanson, G.N., 1990. Calculation of simultaneous isotopic and trace element
744 variations during water-rock interaction with applications to carbonate diagenesis.
745 Geochim. Cosmochim. Acta 54, 3123–3137. https://doi.org/10.1016/0016-7037(90)90128-8
746 Bartley, J.K., Kah, L.C., 2004. Marine carbon reservoir, Corg-Ccarb coupling, and the evolution
747 of the Proterozoic carbon cycle. Geology 32, 129. https://doi.org/10.1130/G19939.1
748 Bartley, J.K., Semikhatov, M.A., Kaufman, A.J., Knoll, A.H., Pope, M.C., Jacobsen, S.B., 2001.
749 Global events across the Mesoproterozoic-Neoproterozoic boundary: C and Sr isotopic

evidence from Siberia. Precambrian Res. 111, 165–202. https://doi.org/10.1016/S0301-9268(01)00160-7

Baumgartner, L.K., Reid, R.P., Dupraz, C., Decho, A.W., Buckley, D.H., Spear, J.R., Przekop, K.M., Visscher, P.T., 2006. Sulfate reducing bacteria in microbial mats: Changing paradigms, new discoveries. Sediment. Geol. 185, 131–145. https://doi.org/10.1016/J.SEDGEO.2005.12.008

Berner, R.A., Scott, M.R., Thomlinson, C., 1970. Carbonate alkalinity in the pore waters of anoxic marine sediments. Limnol. Oceanogr. 15, 544–549. https://doi.org/10.4319/lo.1970.15.4.0544

Bottrell, S.H., Newton, R.J., 2006. Reconstruction of changes in global sulfur cycling from marine sulfate isotopes. Earth-Science Rev. 75, 59–83. https://doi.org/10.1016/J.EARSCIREV.2005.10.004

Brand, U., Veizer, J., 1980. Chemical Diagenesis of a Multicomponent Carbonate System--1: Trace Elements. SEPM J. Sediment. Res. Vol. 50, 1219–1236. https://doi.org/10.1306/212F7BB7-2B24-11D7-8648000102C1865D

Brett, C.E., Boucot, A.J., Jones, B., 1993. Absolute depths of Silurian benthic assemblages. Lethaia 26, 25–40. https://doi.org/10.1111/j.1502-3931.1993.tb01507.x

Bryant, R.N., Jones, C., Raven, M.R., Gomes, M.L., Berelson, W.M., Bradley, A.S., Fike, D.A., 2019. Sulfur isotope analysis of microcrystalline iron sulfides using secondary ion mass spectrometry imaging: Extracting local paleo-environmental information from modern and ancient sediments. Rapid Commun. Mass Spectrom. 33, 491–502. https://doi.org/10.1002/rcm.8375

Bryant, R.N., Jones, C., Raven, M.R., Owens, J.D., Fike, D.A., 2020. Shifting modes of iron

773 sulfidization at the onset of OAE-2 drive regional shifts in pyrite δ34S records. Chem. Geol.
774 553, 119808. https://doi.org/10.1016/j.chemgeo.2020.119808
775 Burdett, J.W., Arthur, M.A., Richardson, M., 1989. A Neogene seawater sulfur isotope age curve
776 from calcareous pelagic microfossils. Earth Planet. Sci. Lett. 94, 189–198.
777 https://doi.org/10.1016/0012-821X(89)90138-6
778 Calner, M., 2008. Silurian global events – at the tipping point of climate change, in: Mass
779 Extinction. Springer Berlin Heidelberg, Berlin, Heidelberg, pp. 21–57.
780 https://doi.org/10.1007/978-3-540-75916-4_4
781 Canfield, D.E., 2001. Biogeochemistry of sulfur isotopes. Stable Isot. Geochemistry 43, 607–
782 636. https://doi.org/10.1515/9781501508745-015
783 Canfield, D.E., Raiswell, R., Westrich, J.T., Reaves, C.M., Berner, R.A., 1986. The use of
784 chromium reduction in the analysis of reduced inorganic sulfur in sediments and shales.
785 Chem. Geol. 54, 149–155. https://doi.org/10.1016/0009-2541(86)90078-1
786 Chester, R., 1990. Trace elements in the oceans, in: Marine Geochemistry. Springer Netherlands,
787 pp. 346–421. https://doi.org/10.1007/978-94-010-9488-7_11
788 Chiba, H., Sakai, H., 1985. Oxygen isotope exchange rate between dissolved sulfate and water at
789 hydrothermal temperatures. Geochim. Cosmochim. Acta 49, 993–1000.
790 https://doi.org/10.1016/0016-7037(85)90314-X
791 Christ, N., Immenhauser, A., Wood, R.A., Darwich, K., Niedermayr, A., 2015. Petrography and
792 environmental controls on the formation of Phanerozoic marine carbonate hardgrounds.
793 Earth-Science Rev. 151, 176–226. https://doi.org/10.1016/J.EARSCIREV.2015.10.002
794 Claypool, G.E., 2004. Ventilation of marine sediments indicated by depth profiles of pore water
795 sulfate and δ34S. Geochemical Soc. Spec. Publ. 9, 59–65. https://doi.org/10.1016/S1873-

9881(04)80007-5

Cocks, L.R.M., Torsvik, T.H., 2005. Baltica from the late Precambrian to mid-Palaeozoic times: The gain and loss of a terrane's identity. Earth-Science Rev. 72, 39–66. https://doi.org/10.1016/J.EARSCIREV.2005.04.001

Cramer, B.D., Brett, C.E., Melchin, M.J., Männik, P., Kleffner, M.A., Mclaughlin, P.I., Loydell, D.K., Munnecke, A., Jeppsson, L., Corradini, C., Brunton, F.R., Saltzman, M.R., 2011. Revised correlation of Silurian Provincial Series of North America with global and regional chronostratigraphic units and δ13Ccarb chemostratigraphy. Lethaia 44, 185–202. https://doi.org/10.1111/j.1502-3931.2010.00234.x

Cramer, B.D., Loydell, D.K., Samtleben, C., Munnecke, A., Kaljo, D., Männik, P., Martma, T., Jeppsson, L., Kleffner, M.A., Barrick, J.E., Johnson, C.A., Emsbo, P., Joachimski, M.M., Bickert, T., Saltzman, M.R., 2010. Testing the limits of Paleozoic chronostratigraphic correlation via high-resolution (<500 k.y.) integrated conodont, graptolite, and carbon isotope (δ13Ccarb) biochemostratigraphy across the llandovery-Wenlock (Silurian) boundary: Is a unified Phanerozoic. Bull. Geol. Soc. Am. 122, 1700–1716. https://doi.org/10.1130/B26602.1

Cramer, B.D., Saltzman, M.R., 2005. Sequestration of 12C in the deep ocean during the early Wenlock (Silurian) positive carbon isotope excursion. Palaeogeogr. Palaeoclimatol. Palaeoecol. 219, 333–349. https://doi.org/10.1016/J.PALAEO.2005.01.009

Eldridge, D.L., Guo, W., Farquhar, J., 2016. Theoretical estimates of equilibrium sulfur isotope effects in aqueous sulfur systems: Highlighting the role of isomers in the sulfite and sulfoxylate systems. Geochim. Cosmochim. Acta 195, 171–200. https://doi.org/10.1016/J.GCA.2016.09.021

819 Erhardt, A.M., Turchyn, A. V., Dickson, J.A.D., Sadekov, A.Y., Taylor, P.D., Wilson, M.A.,
820 Scott, P., Schrag, D.P., 2020. Chemical Composition of Carbonate Hardground Cements as
821 Reconstructive Tools for Phanerozoic Pore Fluids. Geochemistry, Geophys. Geosystems 21.
822 https://doi.org/10.1029/2019GC008448
823 Fichtner, V., Strauss, H., Immenhauser, A., Buhl, D., Neuser, R.D., Niedermayr, A., 2017.
824 Diagenesis of carbonate associated sulfate. Chem. Geol. 463, 61–75.
825 https://doi.org/10.1016/J.CHEMGEO.2017.05.008
826 Fike, D.A., Bradley, A.S., Rose, C. V., 2015. Rethinking the Ancient Sulfur Cycle. Annu. Rev.
827 Earth Planet. Sci. 43, 593–622. https://doi.org/10.1146/annurev-earth-060313-054802
828 Fölling, P.G., Frimmel, H.E., 2002. Chemostratigraphic correlation of carbonate successions in
829 the Gariep and Saldania Belts, Namibia and South Africa. Basin Res. 14, 69–88.
830 https://doi.org/10.1046/j.1365-2117.2002.00167.x
831 Garrels, R.M., Lerman, A., 1981. Phanerozoic cycles of sedimentary carbon and sulfur
832 (isotopes/sediment cycles/natural oxygen reservoirs). Geology 78, 4652–4656.
833 Geyman, E.C., Maloof, A.C., Dyer, B., 2021. How is sea level change encoded in carbonate
834 stratigraphy? Earth Planet. Sci. Lett. 560, 116790.
835 https://doi.org/10.1016/j.epsl.2021.116790
836 Gill, B.C., Lyons, T.W., Frank, T.D., 2008. Behavior of carbonate-associated sulfate during
837 meteoric diagenesis and implications for the sulfur isotope paleoproxy. Geochim.
838 Cosmochim. Acta 72, 4699–4711. https://doi.org/10.1016/J.GCA.2008.07.001
839 Gill, B.C., Lyons, T.W., Saltzman, M.R., 2007. Parallel, high-resolution carbon and sulfur
840 isotope records of the evolving Paleozoic marine sulfur reservoir. Palaeogeogr.
841 Palaeoclimatol. Palaeoecol. 256, 156–173. https://doi.org/10.1016/J.PALAEO.2007.02.030

842 Goldberg, T., Poulton, S.W., Strauss, H., 2005. Sulphur and oxygen isotope signatures of late
843 Neoproterozoic to early Cambrian sulphate, Yangtze Platform, China: Diagenetic
844 constraints and seawater evolution. Precambrian Res. 137, 223–241.
845 https://doi.org/10.1016/J.PRECAMRES.2005.03.003
846 Gómez Peral, L.E., Poiré, D.G., Strauss, H., Zimmermann, U., 2007. Chemostratigraphy and
847 diagenetic constraints on Neoproterozoic carbonate successions from the Sierras Bayas
848 Group, Tandilia System, Argentina. Chem. Geol. 237, 109–128.
849 https://doi.org/10.1016/j.chemgeo.2006.06.022
850 Halverson, G.P., Dudás, F.Ö., Maloof, A.C., Bowring, S.A., 2007. Evolution of the 87Sr/86Sr
851 composition of Neoproterozoic seawater. Palaeogeogr. Palaeoclimatol. Palaeoecol. 256,
852 103–129. https://doi.org/10.1016/J.PALAEO.2007.02.028
853 Higgins, J.A., Blättler, C.L., Lundstrom, E.A., Santiago-Ramos, D.P., Akhtar, A.A., Crüger
854 Ahm, A.-S., Bialik, O., Holmden, C., Bradbury, H., Murray, S.T., Swart, P.K., 2018.
855 Mineralogy, early marine diagenesis, and the chemistry of shallow-water carbonate
856 sediments. Geochim. Cosmochim. Acta 220, 512–534.
857 https://doi.org/10.1016/J.GCA.2017.09.046
858 Hints, O., Killing, M., Männik, P., Nestor, V., 2006. Frequency patterns of chitinozoans,
859 scolecodonts, and conodonts in the upper Llandovery and lower Wenlock of the Paatsalu
860 core, western Estonia. Proc. Est. Acad. Sci. Geol. 55, 128–155.
861 Husson, J.M., Higgins, J.A., Maloof, A.C., Schoene, B., 2015. Ca and Mg isotope constraints on
862 the origin of Earth's deepest δ13C excursion. Geochim. Cosmochim. Acta 160, 243–266.
863 https://doi.org/10.1016/J.GCA.2015.03.012
864 Jeppsson, L., 1997. The anatomy of the mid-Early Silurian Ireviken Event and a Scenario of P-S

Events, in: Paleontological Events: Stratigraphic, Ecological and Evolutionary Implications. pp. 451–492.

Johnson, D.L., Grossman, E.L., Webb, S.M., Adkins, J.F., 2020. Brachiopod δ34SCAS microanalyses indicate a dynamic, climate-influenced Permo-Carboniferous sulfur cycle. Earth Planet. Sci. Lett. 546, 116428. https://doi.org/10.1016/j.epsl.2020.116428

Jones, D.S., Brothers, R.W., Ahm, A.-S.C., Slater, N., Higgins, J.A., Fike, D.A., 2019. Sea level, carbonate mineralogy, and early diagenesis controlled δ13C records in Upper Ordovician carbonates. Geology. https://doi.org/10.1130/g46861.1

Jones, D.S., Fike, D.A., 2013. Dynamic sulfur and carbon cycling through the end-Ordovician extinction revealed by paired sulfate–pyrite δ34S. Earth Planet. Sci. Lett. 363, 144–155. https://doi.org/10.1016/j.epsl.2012.12.015

Kah, L.C., Lyons, T.W., Frank, T.D., 2004. Low marine sulphate and protracted oxygenation of the Proterozoic biosphere. Nature 431, 834–838. https://doi.org/10.1038/nature02974

Kaljo, D., Martma, T., 2006. Application of carbon isotope stratigraphy to dating the Baltic Silurian rocks. GFF 128, 123–129. https://doi.org/10.1080/11035890601282123

Kaljo, D., Martma, T., 2000. Carbon isotopic composition of Llandovery rocks (East Baltic Silurian) with environmental interpretation, in: Proceedings of the Estonian Academy of Sciences, Geology. pp. 267–283.

Kampschulte, A., Strauss, H., 2004. The sulfur isotopic evolution of Phanerozoic seawater based on the analysis of structurally substituted sulfate in carbonates. Chem. Geol. 204, 255–286. https://doi.org/10.1016/J.CHEMGEO.2003.11.013

Kiipli, E., Kiipli, T., Kallaste, T., 2006. Identification of the O-bentonite in the deep shelf sections with implication on stratigraphy and lithofacies, East Baltic Silurian. GFF 128,

255–260. https://doi.org/10.1080/11035890601283255

Kiipli, T., Orlova, K., Kiipli, E., Kallaste, T., 2008. Use of immobile trace elements for the correlation of Telychian bentonites on Saaremaa Island, Estonia, and mapping of volcanic ash clouds. Est. J. Earth Sci. 57, 39–52. https://doi.org/10.3176/earth.2008.1.04

Kozik, N.P., Young, S.A., Bowman, C.N., Saltzman, M.R., Them, T.R., 2019. Middle–Upper Ordovician (Darriwilian–Sandbian) paired carbon and sulfur isotope stratigraphy from the Appalachian Basin, USA: Implications for dynamic redox conditions spanning the peak of the Great Ordovician Biodiversification Event. Palaeogeogr. Palaeoclimatol. Palaeoecol. 520, 188–202. https://doi.org/10.1016/j.palaeo.2019.01.032

Kump, L.R., Arthur, M.A., 1999. Interpreting carbon-isotope excursions: carbonates and organic matter. Chem. Geol. 161, 181–198. https://doi.org/10.1016/S0009-2541(99)00086-8

Lehnert, O., Männik, P., Joachimski, M.M., Calner, M., Frýda, J., 2010. Palaeoclimate perturbations before the Sheinwoodian glaciation: A trigger for extinctions during the 'Ireviken Event.' Palaeogeogr. Palaeoclimatol. Palaeoecol. 296, 320–331. https://doi.org/10.1016/j.palaeo.2010.01.009

Liu, Xi, Deng, W., Wei, G., 2019. Carbon and oxygen isotopic analyses of calcite in calcite–dolomite mixtures: Optimization of selective acid extraction. Rapid Commun. Mass Spectrom. 33, 411–418. https://doi.org/10.1002/rcm.8365

Liu, Xiting, Fike, D., Li, A., Dong, J., Xu, F., Zhuang, G., Rendle-Bühring, R., Wan, S., 2019. Pyrite sulfur isotopes constrained by sedimentation rates: Evidence from sediments on the East China Sea inner shelf since the late Pleistocene. Chem. Geol. 505, 66–75. https://doi.org/10.1016/j.chemgeo.2018.12.014

Lowenstein, T.K., Hardie, L.A., Timofeeff, M.N., Demicco, R. V., 2003. Secular variation in

seawater chemistry and the origin of calcium chloride basinal brines. Geology 31, 857. https://doi.org/10.1130/G19728R.1

Loydell, D.K., Nestor, V., Mnnik, P., 2010. Integrated biostratigraphy of the lower silurian of the Kolka-54 core, Latvia. Geol. Mag. 147, 253–280. https://doi.org/10.1017/S0016756809990574

Männik, P., Põldvere, A., Nestor, V., Kallaste, T., Kiipli, T., Martma, T., 2014. The Llandovery-Wenlock boundary interval in west-central continental Estonia: an example from the Suigu (S-3) core section. Est. J. Earth Sci. 63, 1–17. https://doi.org/10.3176/earth.2014.01

Marenco, P.J., Corsetti, F.A., Hammond, D.E., Kaufman, A.J., Bottjer, D.J., 2008a. Oxidation of pyrite during extraction of carbonate associated sulfate. Chem. Geol. 247, 124–132. https://doi.org/10.1016/j.chemgeo.2007.10.006

Marenco, P.J., Corsetti, F.A., Kaufman, A.J., Bottjer, D.J., 2008b. Environmental and diagenetic variations in carbonate associated sulfate: An investigation of CAS in the Lower Triassic of the western USA. Geochim. Cosmochim. Acta 72, 1570–1582. https://doi.org/10.1016/j.gca.2007.10.033

Munnecke, A., Calner, M., Harper, D.A.T., Servais, T., 2010. Ordovician and Silurian sea–water chemistry, sea level, and climate: A synopsis. Palaeogeogr. Palaeoclimatol. Palaeoecol. 296, 389–413. https://doi.org/10.1016/j.palaeo.2010.08.001

Munnecke, A., Samtleben, C., Bickert, T., 2003. The Ireviken Event in the lower Silurian of Gotland, Sweden – relation to similar Palaeozoic and Proterozoic events. Palaeogeogr. Palaeoclimatol. Palaeoecol. 195, 99–124. https://doi.org/10.1016/S0031-0182(03)00304-3

Nestor, H., Einasto, R., 1997. Ordovician and Silurian Carbonate sedimentation basin, in: Geology and Mineral Resources of Estonia. Estonian Academy Publishers, Tallinn, pp.

192–204.

Nestor, V., 2010. Distribution of Silurian chitinozoans. Viki Drill Core. Est. Geol. Sect. Bulletin 1, 19–20.

Newton, R.J., Pevitt, E.L., Wignall, P.B., Bottrell, S.H., 2004. Large shifts in the isotopic composition of seawater sulphate across the Permo-Triassic boundary in northern Italy. Earth Planet. Sci. Lett. 218, 331–345. https://doi.org/10.1016/S0012-821X(03)00676-9

Pasquier, V., Sansjofre, P., Rabineau, M., Revillon, S., Houghton, J., Fike, D.A., 2017. Pyrite sulfur isotopes reveal glacial−interglacial environmental changes. Proc. Natl. Acad. Sci. 114, 5941–5945. https://doi.org/10.1073/pnas.1618245114

Paytan, A., 1998. Sulfur Isotopic Composition of Cenozoic Seawater Sulfate. Science (80-.). 282, 1459–1462. https://doi.org/10.1126/science.282.5393.1459

Percak-Dennett, E., He, S., Converse, B., Konishi, H., Xu, H., Corcoran, A., Noguera, D., Chan, C., Bhattacharyya, A., Borch, T., Boyd, E., Roden, E.E., 2017. Microbial acceleration of aerobic pyrite oxidation at circumneutral pH. Geobiology 15, 690–703. https://doi.org/10.1111/gbi.12241

Present, T.M., 2018. Controls on the Sulfur Isotopic Composition of Carbonate-Associated Sulfate. California Institute of Technology.

Present, T.M., Adkins, J.F., Fischer, W.W., 2020. Variability in Sulfur Isotope Records of Phanerozoic Seawater Sulfate. Geophys. Res. Lett. 47. https://doi.org/10.1029/2020GL088766

Present, T.M., Gutierrez, M., Paris, G., Kerans, C., Grotzinger, J.P., Adkins, J.F., 2019. Diagenetic controls on the isotopic composition of carbonate-associated sulphate in the Permian Capitan Reef Complex, West Texas. Sedimentology 66, 2605–2626.

https://doi.org/10.1111/sed.12615

Present, T.M., Paris, G., Burke, A., Fischer, W.W., Adkins, J.F., 2015. Large Carbonate Associated Sulfate isotopic variability between brachiopods, micrite, and other sedimentary components in Late Ordovician strata. Earth Planet. Sci. Lett. 432, 187–198. https://doi.org/10.1016/J.EPSL.2015.10.005

Rennie, V.C.F., Turchyn, A. V., 2014. The preservation of δSSO434 and δOSO418 in carbonate-associated sulfate during marine diagenesis: A 25 Myr test case using marine sediments. Earth Planet. Sci. Lett. 395, 13–23. https://doi.org/10.1016/J.EPSL.2014.03.025

Richardson, J.A., Keating, C., Lepland, A., Hints, O., Bradley, A.S., Fike, D.A., 2019a. Silurian records of carbon and sulfur cycling from Estonia: The importance of depositional environment on isotopic trends. Earth Planet. Sci. Lett. 512, 71–82. https://doi.org/10.1016/j.epsl.2019.01.055

Richardson, J.A., Newville, M., Lanzirotti, A., Webb, S.M., Rose, C. V, Catalano, J.G., Fike, D.A., 2019b. Depositional and Diagenetic Constrains on the Abundance and Spatial Variability of Carbonate-Associated Sulfate. Chem. Geol. 523, 59–72. https://doi.org/10.1016/J.CHEMGEO.2019.05.036

Rose, C. V., Fischer, W.W., Finnegan, S., Fike, D.A., 2019. Records of carbon and sulfur cycling during the Silurian Ireviken Event in Gotland, Sweden. Geochim. Cosmochim. Acta 246, 299–316. https://doi.org/10.1016/j.gca.2018.11.030

Rubel, M., Hints, O., Meidla, T., Nestor, V., Sarv, L., Sibul, I., 2007. Lower Silurian biostratigraphy of the Viirelaid core, western Estonia. Est. J. Earth Sci. 56, 193–204. https://doi.org/10.3176/earth.2007.01

Samtleben, C., Munnecke, A., Bickert, T., 2000. Development of facies and C/O-isotopes in

transects through the Ludlow of Gotland: Evidence for global and local influences on a shallow-marine environment. Facies 43, 1–38. https://doi.org/10.1007/BF02536983

Sim, M.S., Bosak, T., Ono, S., 2011. Large sulfur isotope fractionation does not require disproportionation. Science (80-.). 333, 74–77. https://doi.org/10.1126/science.1205103

Stebbins, A., Algeo, T.J., Olsen, C., Sano, H., Rowe, H., Hannigan, R., 2018. Sulfur-isotope evidence for recovery of seawater sulfate concentrations from a PTB minimum by the Smithian-Spathian transition. Earth-Science Rev. https://doi.org/10.1016/J.EARSCIREV.2018.08.010

Strauss, H., 1997. The isotopic composition of sedimentary sulfur through time. Palaeogeogr. Palaeoclimatol. Palaeoecol. 132, 97–118. https://doi.org/10.1016/S0031-0182(97)00067-9

Swart, P.K., 2015. The geochemistry of carbonate diagenesis: The past, present and future. Sedimentology 62, 1233–1304. https://doi.org/10.1111/sed.12205

Swart, P.K., Eberli, G., 2005. The nature of the δ13C of periplatform sediments: Implications for stratigraphy and the global carbon cycle. Sediment. Geol. 175, 115–129. https://doi.org/10.1016/J.SEDGEO.2004.12.029

Thompson, C.K., Kah, L.C., 2012. Sulfur isotope evidence for widespread euxinia and a fluctuating oxycline in Early to Middle Ordovician greenhouse oceans. Palaeogeogr. Palaeoclimatol. Palaeoecol. 313–314, 189–214. https://doi.org/10.1016/J.PALAEO.2011.10.020

Tonarová, P., Hints, O., Eriksson, M.E., 2014. Impact of the Silurian Ireviken Event on polychaete faunas: New insights from the Viki drill core, western Estonia. GFF 136, 270–274. https://doi.org/10.1080/11035897.2013.862855

Torsvik, T.H., Cocks, L.R.M., 2013. New global palaeogeographical reconstructions for the

1003 Early Palaeozoic and their generation. Geol. Soc. Mem. 38, 5–24.
1004 https://doi.org/10.1144/M38.2
1005 Tostevin, R., He, T., Turchyn, A. V., Wood, R.A., Penny, A.M., Bowyer, F., Antler, G., Shields,
1006 G.A., 2017. Constraints on the late Ediacaran sulfur cycle from carbonate associated sulfate.
1007 Precambrian Res. 290, 113–125. https://doi.org/10.1016/j.precamres.2017.01.004
1008 Trotter, J.A., Williams, I.S., Barnes, C.R., Männik, P., Simpson, A., 2016. New conodont δ18O
1009 records of Silurian climate change: Implications for environmental and biological events.
1010 Palaeogeogr. Palaeoclimatol. Palaeoecol. 443, 34–48.
1011 https://doi.org/10.1016/j.palaeo.2015.11.011
1012 Turchyn, A. V., Schrag, D.P., 2006. Cenozoic evolution of the sulfur cycle: Insight from oxygen
1013 isotopes in marine sulfate. Earth Planet. Sci. Lett. 241, 763–779.
1014 https://doi.org/10.1016/J.EPSL.2005.11.007
1015 Turchyn, A. V., Schrag, D.P., Coccioni, R., Montanari, A., 2009. Stable isotope analysis of the
1016 Cretaceous sulfur cycle. Earth Planet. Sci. Lett. 285, 115–123.
1017 https://doi.org/10.1016/J.EPSL.2009.06.002
1018 Vandenbroucke, T.R.A., Munnecke, A., Leng, M.J., Bickert, T., Hints, O., Gelsthorpe, D.,
1019 Maier, G., Servais, T., 2013. Reconstructing the environmental conditions around the
1020 Silurian Ireviken Event using the carbon isotope composition of bulk and palynomorph
1021 organic matter. Geochemistry, Geophys. Geosystems 14, 86–101.
1022 https://doi.org/10.1029/2012GC004348
1023 Xiao, S., Cui, H., Kang, J., McFadden, K.A., Kaufman, A.J., Kitajima, K., Fournelle, J.H.,
1024 Schwid, M., Nolan, M., Baele, J.-M., Valley, J.W., 2020. Using SIMS to decode noisy
1025 stratigraphic δ13C variations in Ediacaran carbonates. Precambrian Res. 105686.

https://doi.org/10.1016/j.precamres.2020.105686

Young, S.A., Benayoun, E., Kozik, N.P., Hints, O., Martma, T., Bergström, S.M., Owens, J.D., 2020. Marine redox variability from Baltica during extinction events in the latest Ordovician–early Silurian. Palaeogeogr. Palaeoclimatol. Palaeoecol. 554. https://doi.org/10.1016/j.palaeo.2020.109792

Young, S.A., Gill, B.C., Edwards, C.T., Saltzman, M.R., Leslie, S.A., 2016. Middle–Late Ordovician (Darriwilian–Sandbian) decoupling of global sulfur and carbon cycles: Isotopic evidence from eastern and southern Laurentia. Palaeogeogr. Palaeoclimatol. Palaeoecol. 458, 118–132. https://doi.org/10.1016/j.palaeo.2015.09.040

Young, S.A., Kleinberg, A., Owens, J.D., 2019. Geochemical evidence for expansion of marine euxinia during an early Silurian (Llandovery–Wenlock boundary) mass extinction. Earth Planet. Sci. Lett. 513, 187–196. https://doi.org/10.1016/j.epsl.2019.02.023

Tables

Table 1 – average $\delta^{34}S_{CAS}$ and $\delta^{34}S_{pyr}$ values and average sample-to-sample $\delta^{34}S_{CAS}$ and $\delta^{34}S_{pyr}$ values for each formation to assess the variability of sulfur isotope values within a given depositional environment. The number of samples is included beside each formation name. Average sample-to-sample $\delta^{34}S_{pyr}$ is particularly high in the Velise Fm., as this includes an aberrant sample at 74.24 m of -32.38‰. Excluding this sample brings the average sample-to-sample $\delta^{34}S_{pyr}$ down to 8.3‰ in the Velise Fm (given in parentheses). Similarly, the average sample-to-sample $\delta^{34}S_{pyr}$ decreases from 7 to 4.2‰ in the Jaani Formation when excluding samples that belong to the oolite (which is a rapid shallowing environment; again in parentheses).

Figures

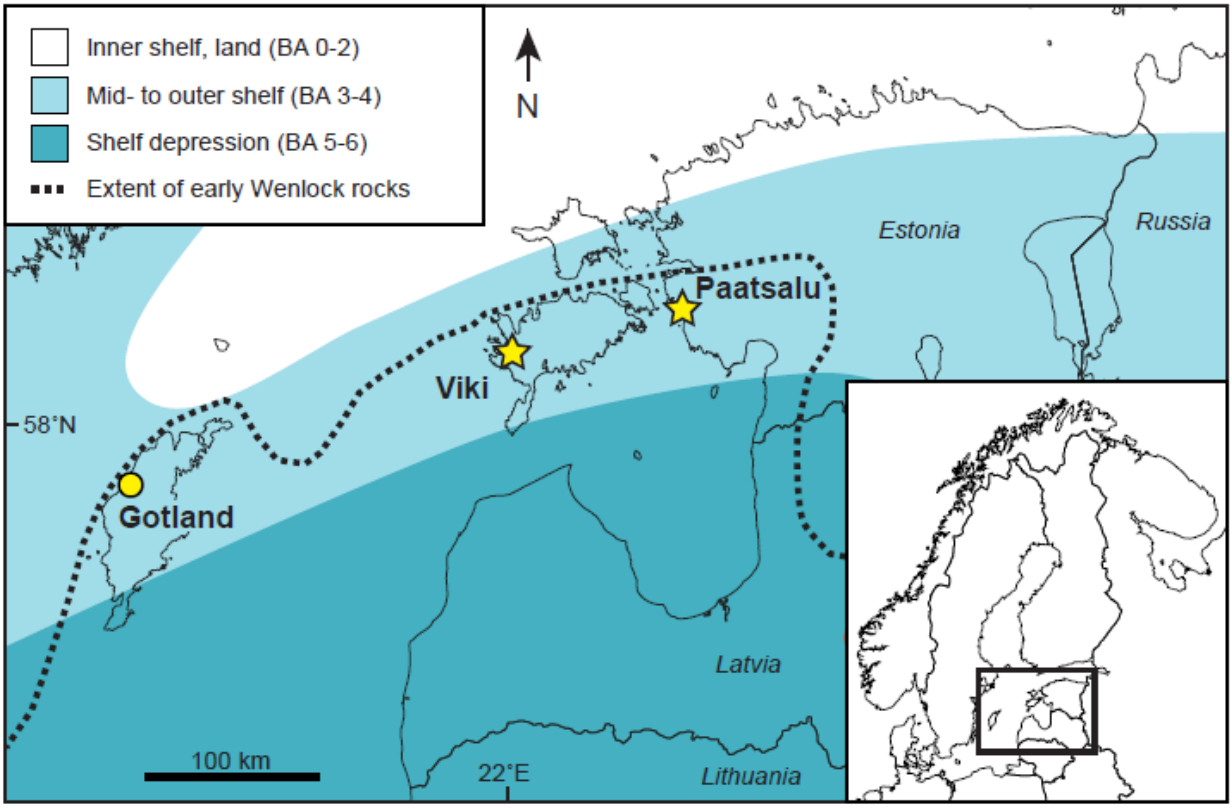

Figure 1 – Map showing the locations of Paatsalu (this study) and Viki drill cores (Richardson et al., 2019a) in Estonia (stars), and a time-equivalent comparison from Gotland Island, Sweden (Rose et al., 2019) (circle). Generalized paleogeography is shown for the early Wenlock (Baarli et al., 2003; Nestor and Einasto, 1997). BA = depth related benthic assemblages (Brett et al., 1993)

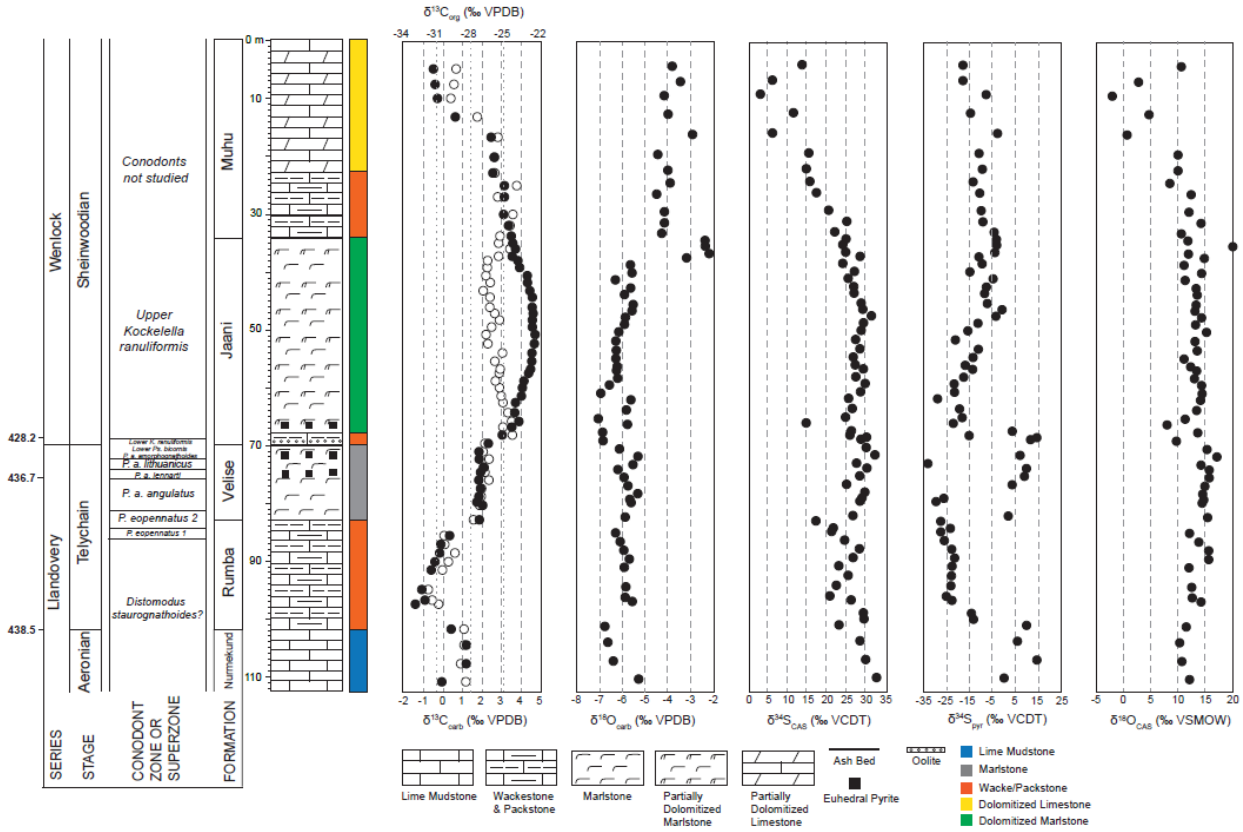

Figure 2 – Paatsalu drill core stratigraphy (left) and coeval isotope chemostratigraphy. From left to right: $\delta^{13}C_{carb}$ (solid circles; dashed lines) and $\delta^{13}C_{org}$ (open circles; dotted lines), $\delta^{18}O_{carb}$, $\delta^{34}S_{CAS}$, $\delta^{34}S_{pyr}$ and $\delta^{18}O_{CAS}$. Note that the same lithofacies color coding is used in subsequent figures.

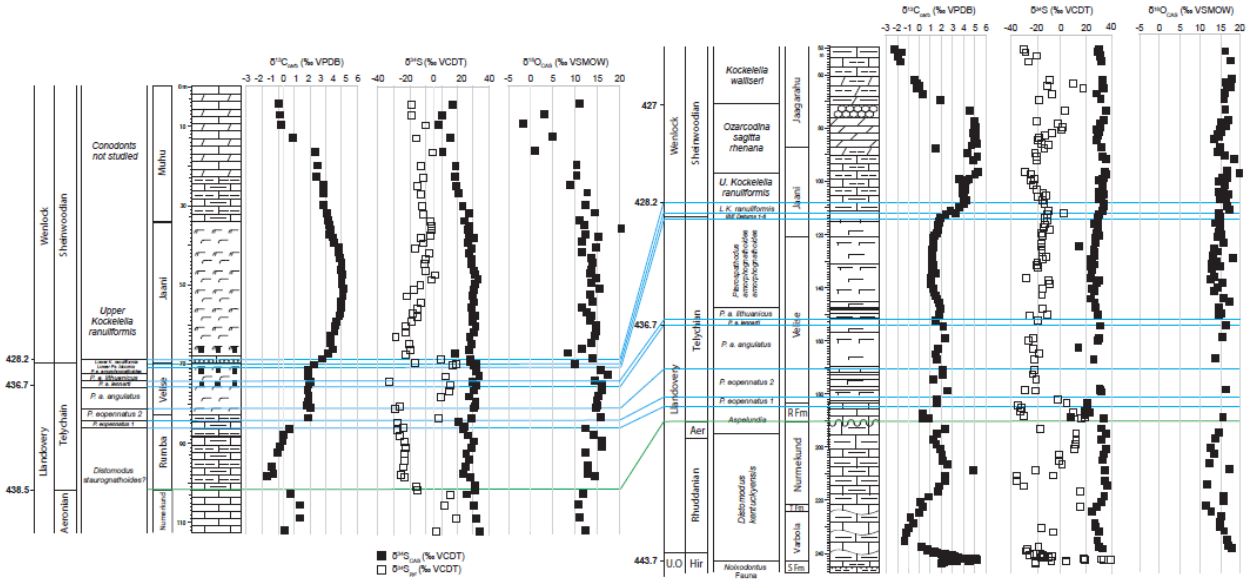

Figure 3 – Comparison of $\delta^{13}C_{carb}$, $\delta^{34}S_{pyr}$, $\delta^{34}S_{CAS}$ (solid squares) and $\delta^{18}O_{CAS}$ (open squares) from Paatsalu (left) and Viki (right; Richardson et al., 2019). Correlations made based on conodont biozones (blue lines) and the top of the *Conochitina alargada* chitinozoan biozone (green line). See Fig. 2 for lithology legend.

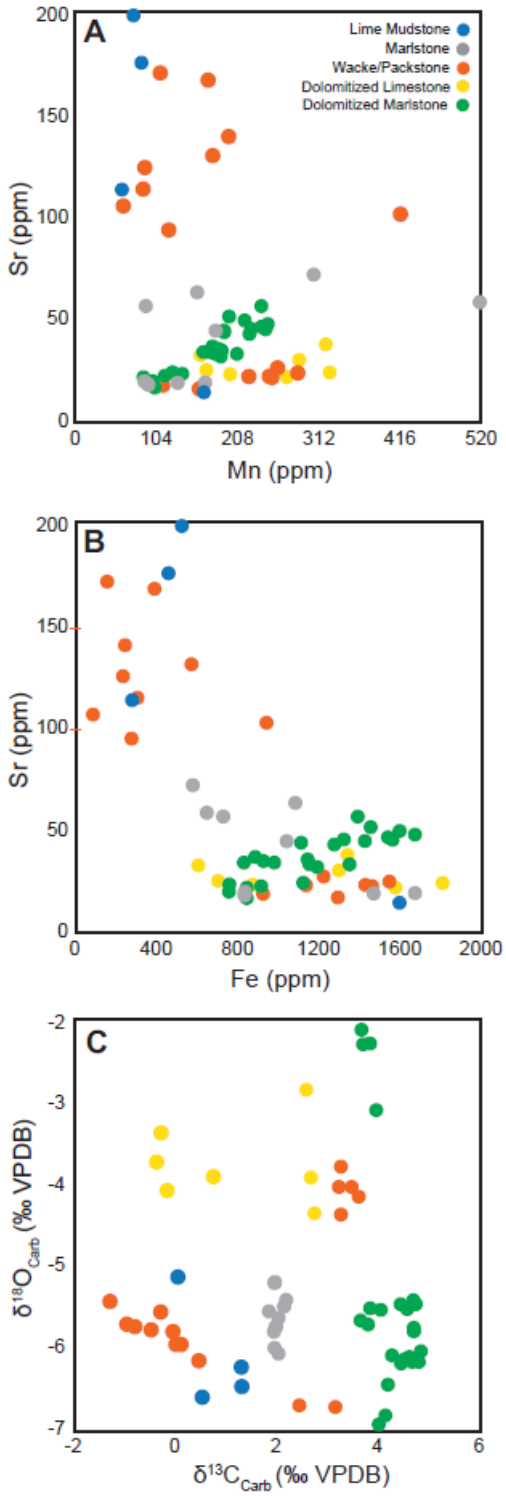

1065

1066 Figure 4 – Cross plots of indicators of post-depositional late-stage diagenesis color-coded by

1067 lithology. (A) Sr vs. Mn abundance, (B) Sr vs. Fe abundance, (C) $\delta^{13}C_{carb}$ vs. $\delta^{18}O_{carb}$,

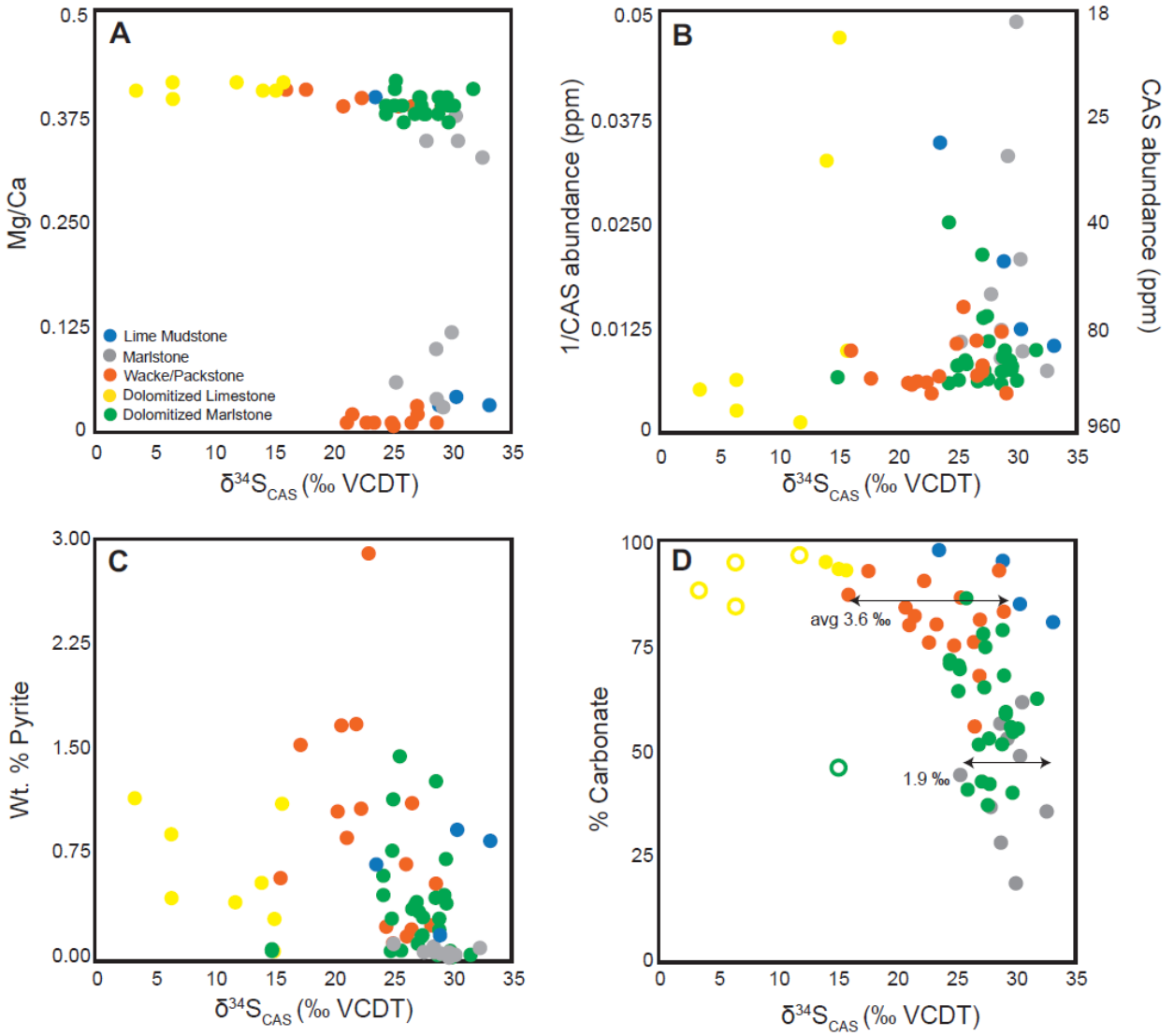

Figure 5 – Cross plots of $\delta^{34}S_{CAS}$ vs. (A) Mg/Ca molar ratio, (B) 1/CAS abundance, (C) wt % S in pyrite and (D) carbonate abundance. Open symbols are samples thought to be altered. Arrows represent the average sample-to-sample variability in shallow-water (3.6‰) and deep-water (1.9‰) facies.

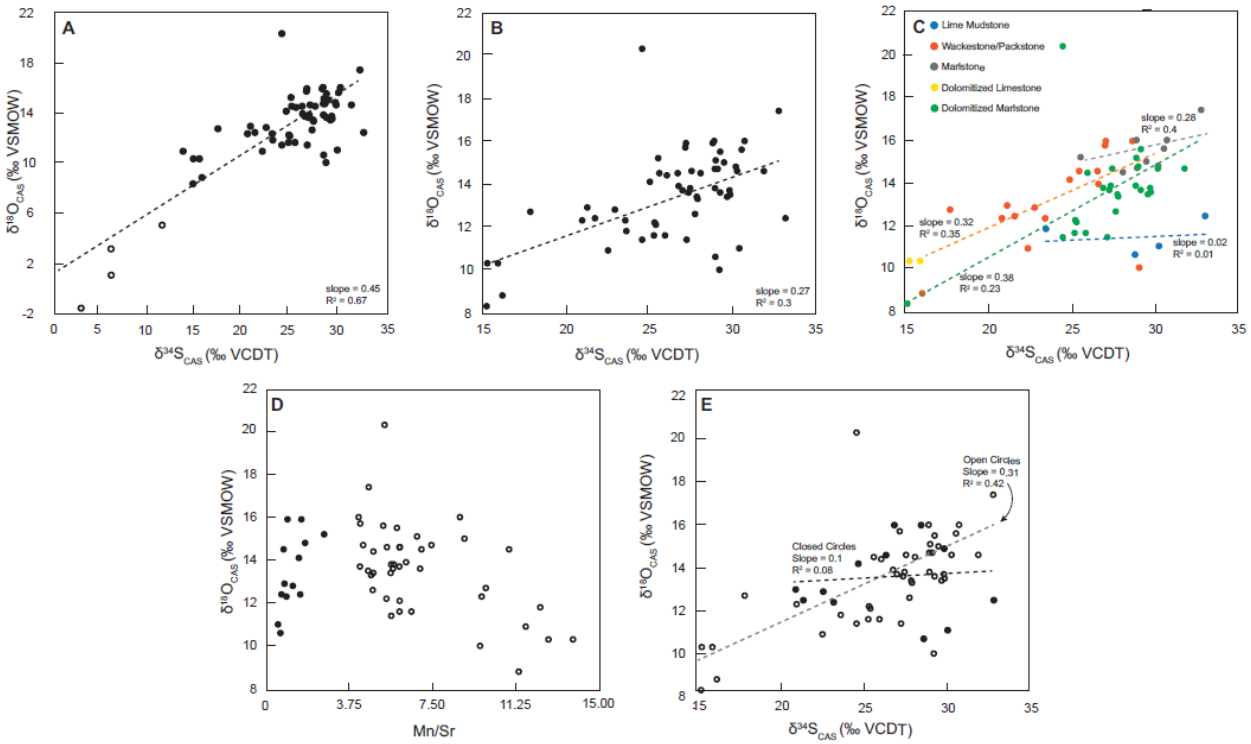

1073

1074 Figure 6 – Cross plots of $\delta^{18}O_{CAS}$ from the Paatsalu drill core vs. (A) $\delta^{34}S_{CAS}$ with altered samples
1075 as open circles, (B) $\delta^{34}S_{CAS}$ with altered samples shown in A removed, (C) $\delta^{34}S_{CAS}$ color-coded
1076 with lithologic information. The slope for dolomitized limestone is omitted due to the small
1077 number of samples from this unit (n = 2) (D) Mn/Sr. Open circles are samples with Mn/Sr > 4 and
1078 solid circles are samples with Mn/Sr < 4. (E) $\delta^{34}S_{CAS}$ plotted as Mn/Sr > 4 (open circles, grey
1079 dashed line) and Mn/Sr < 4 (solid circles, black dashed line).

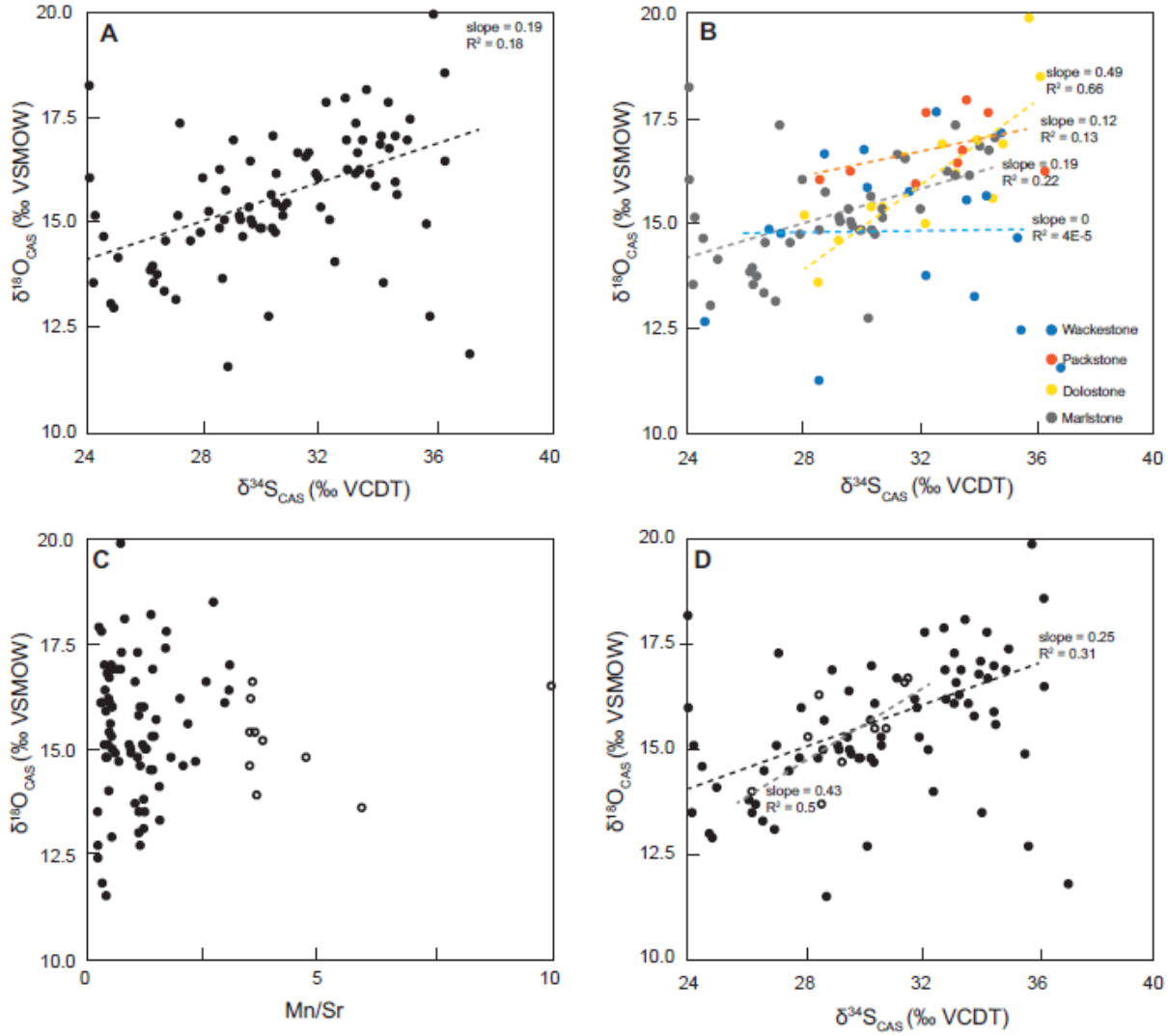

1080

1081 Figure 7 - Cross plots of $\delta^{18}O_{CAS}$ from the Viki drill core vs. (A) $\delta^{34}S_{CAS}$, (B) $\delta^{34}S_{CAS}$ color-coded

1082 with lithologic information, (C) Mn/Sr. Open circles are samples with an Mn/Sr > 4 and solid

1083 circles are samples with Mn/Sr < 4. (D) $\delta^{34}S_{CAS}$ plotted as Mn/Sr > 4 (open circles) and Mn/Sr <

1084 4 (solid circles).

1085
1086